12-2022

A study on Interactions Between Metal-organic Frameworks and Biological Materials

Josh Phipps
University of Arkansas, Fayetteville

A Study on Interactions Between Metal-organic Frameworks and Biological Materials

A dissertation submitted in partial fulfillment
of the requirements for the degree of
Doctor of Philosophy in Cell and Molecular Biology

by

Joshua Phipps
Southwest Baptist University
Bachelor of Science in Biology 2016

December 2022
University of Arkansas

This dissertation is approved for recommendation to the Graduate Council.

_____
Jorge Almodóvar, Ph.D.
Dissertation Director

_____
Jackson Lay, Ph.D.
Committee Member

_____
Chenguan Fan, Ph.D.
Committee Member

_____
Mahmoud Moradi, Ph.D.
Committee Member

_____
Bob Beitle, Ph.D.
Committee Member

Abstract

Metal-organic frameworks or MOFs are an extremely useful tool in many areas of applications. Their popularity in recent years has arisen from their high efficiency in catalytic chemical reactions. This is made possible due to their porous interior and the ability of the MOFs components to be functionalized. These same traits make MOFs excellent for use in protein encapsulation or immobilization and have the potential to become excellent drug carriers. Their development in this utilization has been limited dramatically compared to MOFs chemical applications. This is due in part to the nature of biological processes taking longer to study, but it is also in part due to a lack of understanding in how biological materials interact with these nanoparticles. In order for the development of biological applications with MOFs to continue, these interactions must be further understood through research. In this compilation of our work, we seek to push the boundaries of conventional understanding in our field by studying the interaction between MOFs and biological materials such as proteins and drugs. In doing so, we report our findings and show that protein loading can possibly be improved, enzyme reactions can be improved outside of normal conditions, cell signaling proteins can be delivered successfully to cells and illicit a cellular response, and MOF particles can be effectively used as a delivery device to provide sustained and controlled release of both guest particles and drugs conjugated to the exterior of the MOF particle.

Table of Contents

ii.0 Introduction 1
2.0 Chapter 1: Catalytic Activity, Stability, and Loading Trends of Alcohol Dehydrogenase Enzyme Encapsulated in a Metal-Organic Framework 8
2.0.1 Abstract 8
2.0.2 Introduction 9
2.1.0 Experimental Section 12
2.1.1 Synthesis of ADH 12
2.1.2 Synthesis of PCN-333(Fe) 13
2.1.3 Encapsulation of ADH in PCN-333(Fe) 13
2.1.4 Activity measurement of ADH@PCN-333(Fe) 14
2.1.5 Effect of temperature on activity of ADH@PCN-333(Fe) 15
2.1.6 Effect of pH on activity of ADH@PCN-333(Fe) 15
2.1.7 Effect of solvent on activity of ADH@PCN-333(Fe) 16
2.1.8 Stability of ADH@PCN-333(Fe) 16
2.1.9 Recyclability of ADH@PCN-333(Fe) 16
2.1.10 GC-MS analysis 17
2.1.11 Statistical analysis 17
2.2.0 Results and discussion 17
2.2.1 Encapsulation of ADH in PCN-333. 17
2.2.2 Stability of ADH@PCN-333 over time 22
2.2.3 Effect of pH on ADH@PCN-333 activity 26
2.2.4 Effect of solvent on the activity of ADH@PCN-333 28
2.2.5 Effect of temperature on ADH@PCN-333 activity 29
2.2.6 Recyclability of ADH@PCN-333 30
2.2.7 Confirmation of the product 30
2.3.0 Conclusions from experiment 31
3.0 Chapter 2: A study on the effectiveness of PCN-333(Fe) as a drug delivery device for IFN-γ and its effect on Human Kupfer Cell Viability 38
3.0.1 Abstract 38
3.0.2 Introduction 39

3.1.0 Experimental Section 42
3.1.1 Synthesis of PCN-333(Fe) 42
3.1.2 Immobilization of IFN-γ with PCN-333(Fe) 43
3.1.3 hMSC Viability 43
3.1.4 Real-time monitoring of hMSCs behavior 45
3.1.5 Immunomodulatory factor expression of hMSC's 45
3.1.6 hMSC Differentiation 46
3.2.0 Results and Discussion 47
3.2.1 Characterization of PCN-333(Fe) 47
3.2.2 Immobilization of IFN-X with PCN-333(Fe) 47
3.2.3 PrestoBlue Viability Assay 48
3.2.4 Real-time monitoring of cell behavior and proliferation 49
3.2.5 IDO Assay 51
3.2.6 Cells differentiation assay 52
3.3.0 Conclusions from experiment 53
4.0 Chapter 3: Layer-by-layer polyelectrolyte coating on Metal-organic Frameworks for use as a drug delivery device 57
4.0.1 Abstract 57
4.0.2 Introduction 58
4.1.0 Experimental Section 60
4.1.1UiO-66 Synthesis 60
4.1.2 Layer-by layer coating of UiO-66 61
4.1.4 Toxicity study: real-time monitoring of human Schwann cells cultured with HEP/PEI coated MOFs supplemented in the culture medium. 62
4.2.0 Results & Discussion 63
4.2.1 UiO-66 characterization and coating. 63
4.2.2 Toxicity test 65
4.3.0 Chapter Conclusion 69
5.0 Conclusion 74
6.0 Bibliography ..... **Error! Bookmark not defined.**

List of Publications

- Chapter 1

    - J. Phipps, H. Chen, C. Donovan, D. Dominguez, S. Morgan, B. Weidman, C. Fan, and H. Beyzavi. ACS Appl. Mater. Interfaces, 2020 DOI: 10.1021/acsami.0c0696 Catalytic Activity, Stability, and Loading Trends of Alcohol Dehydrogenase Enzyme Encapsulated in a Metal-Organic Framework. Status: Published.

- Chapter 2

    - J. Phipps, M. Haseli, B. Wilson, J. Corbitt, and J. Almodóvar. Submitted to ACS Appl. Mater. Interfaces. April 2022. A study on the effectiveness of PCN-333(Fe) as a drug delivery device for IFN-γ and its effect on Human Kupfer Cell Viability. Status: Submitted.

- Chapter 3

    - J. Phipps, L. Pinzon-Herrera, B. Wilson, J. Almodóvar. Submitted to ACS Appl. Mater. Interfaces. April 2022. Layer-by-layer polyelectrolyte coating on Metal-organic Frameworks for their use as a drug delivery device. Status: Submitted.

1.0 Introduction

There are many intersections between the science of Chemistry and Biology. That statement has never been truer as in the last century as the unraveling of the foundations of Biology led straight to principles of chemistry.[1] The most significant connection debatably being the discovery of the alpha helix by Franklin, Watson, and Crick.[2] This groundbreaking discovery led to the genetic revolution where the mindset of human existence changed from the understanding that people are not only shaped by their environment, toward the idea that we as beings are more so trapped; pinned to a given direction in life by the random assortment of base pairs and the library of their genetic code.[3]

The development of genetic theory and the research surrounding it has led to the ability of researchers to now synthesize artificial proteins.[4] This term "artificial" referring to proteins that are either not found in nature or were not originally produced by a given organism. This has led to the recent development of the first ever wide-scaled vaccine production of the spike protein of SARS Cov-2.[5] This being the first instance a modern vaccine has utilized a patient's own body to synthesize a targeted protein in order to induce an immune response.[6] This development, although controversial among some groups. Is a major advancement in the work of biological science.[7]

In order to better understand what proteins are and why they are important, we will need to discuss some of their foundational principles. Proteins come with many different shapes, sizes, and functions. These functions can range from something as integral as a protein like DNA Helicase. The protein responsible for separating DNA into single strands so that it can be copied and without with, no proteins would be made.[8] Alternatively, a protein can be simple as being a

building block of the cell like that of tubulin. A protein found in the tubules of the cell which act as a framework allowing the cell to retain its shape.[9] While there are many other functions of enzymes, one of the most prominent roles is that of a catalyst. These proteins, called enzymes, speed up the rate of a given reaction that is crucial to the cell and otherwise would occur at such a slow rate that the cell typically would not be able to function. These enzymes have been some of the most difficult to understand as slight differences in their coding can lead to complete inactivation. This occurs because of the specificity of an area on the enzyme called the "active site." This location is where all the processes inside the enzyme occur that are relevant to the overall action of the enzyme and is created by the specific folding of the enzyme which can be very different depending on the enzyme being observed.[10] This is why it is said that function follows shape in proteins. Researchers have been able to duplicate and manipulate the production of enzymes, studying their effects by changing one or more amino acids in their sequence moving piece by piece in order to understand how each amino acid plays a role in the enzyme's function.[11] This method of discovery has allowed us to better understand how these enzymes work in nature, but also has allowed for their implementation into significant roles in industries.[12]

While the advancements made in protein development have made substantial strides in recent years, these biological wonders have their own disadvantages. Enzymes are in some ways quite fickle. Their effectiveness is heavily reliant upon the surrounding environmental conditions. If the temperature is too hot, the pH is too low/high, or the surrounding solvent has too many organic compounds the protein will denature. When this happens, the protein will lose its shape. This loss of shape is incredibly important for a protein because it is this shape and the

interactions between the protein's neighboring amino acids that provide the function of the protein. Without this, it will inevitably cease to function properly.[13–15] This means that when industrial reactions using enzymes are occurring, much care must be taken in order to keep these micro-scaled tools functioning properly. This care in business terms equates to time and money. In order to get around this significant drawback of using enzymes, researchers have tried manipulating existing enzymes to perform better under an array of conditions.[11] Additionally, the requisition of enzymes from xenophiles, organisms that thrive in extreme conditions, has been identified as a solution.[16] However, this still does not alleviate the unsolvable and inevitable drawback of using enzymes. That being that they have a lifespan. Eventually, all proteins will cease to function at some point and when that happens, they will need to be replaced. I propose that the solution to this dilemma comes with the introduction of another form of synthetic catalyst, or catalyst housing, known as metal-organic frameworks of "MOFs."

MOFs were first introduced in 1990's by Omar Yaghi. A researcher and professor of Chemistry at the University of California at Berkeley.[17] These nano-scaled particles are porous in nature, crystalline in structure, and have an incredible number of diverse functions.[18,19] This type of particle was born out of the development of particles known as "zeolites." These particles are also porous and crystalline, but do not contain the organic linkers found in MOFs.[20] The diverse functionalities of MOFs come from several of their inherent characteristics. MOFs are composed of two components, the first being a metal-ion node and the second being organic linkers. The metal ion node can be comprised of a single metal ion or a cluster, but either must have an inherent positive charge. Alternatively, the organic linkers can be made of nearly any

organic structure, so long as it is symmetrical, and the terminal groups have a negative charge. For the most part, these negatively charged groups are typically carboxylic acid groups. These two groups combine under specific conditions to form a crystal lattice structure of repeating unit cells that have alternating components of ion and linker. The freedom of variability provided by the framework arises from the researcher's ability to manipulate the combinations of linkers and nodes. These different combinations can change the shape, size, surface area, and functionalization of the particle.[17,19,21–23] Having the choice of determining these factors allows for the MOF particles to be "tailor-made" for specific applications.[24] These applications range from gas storage, separations of chemicals, catalysis by MOF, encapsulation of enzymes for catalysis, and drug delivery.[18,19,22,23] As an example, in filtration and/or separations, linkers can be specifically chosen to promote the passage of one particle over another. A good example of this would be the use of M'MOF-2 & M'MOF-3 which uses the attached copper functional group as well as the inherent charge of the linkers to separate ethylene from acetylene.[25] This same trait makes the particles excellent in the storage of gas molecules where instead of separating molecules, the gas particles are trapped inside the framework and are coordinated to the charged functionalized linkers.[26,27] In addition to this porous interior, MOFs have a naturally high surface area allowing for the storage of larger materials. This surface area and pore size can be increased or decreased by expanding or shortening the length of the linkers used. This trait also makes MOFs excellent for the use as a delivery or encapsulating agent.[28–30] The porous interiors of the MOF particles allow for large material like proteins to infiltrate the framework through a process known as post-synthetic encapsulation or PNE. It is understood that due to their fluid nature, proteins unravel and reform as they enter into the

exterior pores of the MOF and continue inside driven by forces of diffusion. The other method of encapsulation is known as DeNovo synthesis or DNE and occurs when a protein is placed in solution with the starting material of a MOF and the framework is built up around the protein, trapping it inside.[28] In both situations, the protein is essentially trapped inside by both physical and chemical forces. The physical framework inhibits the movement of the protein, but the charges found on the framework and the protein itself interact with one another to keep the protein in place. These interactions include hydrogen bonds, London dispersion forces, and dipole-dipole interactions.[28,31–33]

The ability to encapsulate proteins has two added benefits, the protection of the protein from harsh conditions and, more so in the case of smaller proteins, their sustained and controlled release.[28,33,34] The scenario in which proteins are protected has a lot to do with our previous topic on the downsides of enzyme use. These downsides can almost entirely be addressed by the encapsulation of proteins inside a suitable MOF host. When proteins are held inside the framework, it has been shown that the surrounding MOF protects the enzyme from adverse conditions including high temperature, high or low pH, the presence of organic solvents, and the newest form of protection discovered being the protection from immune responses.[28,35,36] The mechanism of how this occurs is not yet well understood. The current working theory is that the surrounding framework holds the protein in place through the aforementioned interactions and prevents it from unfolding or denaturing.[28–30,37] This is extremely important when the protein happens to be an enzyme. In this case, these benefits from the surrounding framework not only protect the enzyme, but also allow for conditions where a given enzyme's reaction would otherwise not progress. Not only do these reactions work under harsh

conditions, but these surrounding conditions can also be optimized to create opportunities for higher yields and reaction rates that would have otherwise not been possible.[30,38] This opens up a new landscape of new possibilities for enzyme reactions.

While this addresses significant downfalls of using proteins, it does not address all the shortcomings. Specifically, may or may not affect the lifespan of a given protein. This detail is still yet to be studied. In this case, MOFs offer another advantage. Given their ability to be functionalized, the unit cell of a MOF can be manipulated in such a way that synthetic active sites, normally found in enzymes, are instead duplicated in the framework.[39] This has already shown to be an advantageous route for catalytic reactions. One recent paper has even showed that MOF-808 in the presence of polyethyleneimine (PEI) can be used as a catalyst to quickly degrade the toxic nerve gas simulant dimethyl 4-nitrophenyl phosphonate and has the potential to be applied to gas mask filters as a defense mechanism.[40] This is just one example, but this catalytic type of application is by far the most popular aspect of MOF use.

The final application that I would like to discuss is that of MOFs as a delivery device. The porous nature of MOFs, their structural rigidity, the ability for researchers to control their size and shape, their ability to be functionalized, and their ability to readily accept conjugation make them excellent for this role.[21,33,41] Recent studies have already determined that many MOFs are not only biocompatible but also, as previously stated, do not elicit an immune response.[42] When introduced into the body, bare MOF particles will enter the cell via endocytosis and will become housed in an endosome. After this, the MOF is brought to lysosomes and is eventually delivered to the Liver and excreted from the body, similar to other drugs.[42–44] In this case, the particles targeting is quite non-specific inside the body. However, with the conjugation of

targeting molecules, MOFs can be directed to specific locations and cells.[45–47] The most common example of this method is the conjugation of targeting molecules on the exterior of the particle, or the exterior of an applied coating on the outside of the MOF particle. A good example of this is the coating of the N3-Bio-MOF-100 with folic acid as a targeting molecule to direct the complex towards cells experiencing symptoms of cancer. In this case the MOF particles were loaded with curcumin, a drug effective in the treatment of cancer.[48] While this is one example, many others combinations of drugs and MOFs have been researcher. However, the use of these complexes in medical practice has not gotten close to beginning.

While the acceptance of MOFs as catalysts was readily accepted by industry, the use of MOFs as delivery devices has made little progress in the field of medicinal chemistry. The major factor behind this lack of advancement despite the benefits that MOFs can bring can be wrapped into one. It's age. With the development of MOFs not being widely practiced until the 2010's, there are simply not many people in the medical field that know about MOFs. In addition, not enough time has passed in order for researchers to have a full enough understanding of MOF interactions and the implications behind their use.[49] It is for this reason that research into MOFs must proceed and needs more attention.

Presently, the list of applications of MOFs continues to grow. Despite their quick acquisition in the field of chemistry, their implementation in the biological sphere has lagged behind significantly. While some of the benefits of MOFs for use in drug delivery and enzyme encapsulation have been shared by researchers, there are many possibilities that are yet to be developed. The impact that these particles have made on the realm of Chemistry and the subsequent effects on the chemical industry has been profound. However, the as yet

undiscovered uses in their biological applications will be felt, not only by corporations, but by individuals the world over. In this paper we seek to push the boundaries of our understanding of MOF and biological interactions in order to bring more attention to the lesser-known drug delivery and enzyme encapsulation applications of MOFs. In doing so, we aim to provide valuable information that have the capacity to have overwhelming impacts in the near future on both the sectors of industry and healthcare.

2.0 Chapter 1: Catalytic Activity, Stability, and Loading Trends of Alcohol Dehydrogenase Enzyme Encapsulated in a Metal-Organic Framework

2.0.1 Abstract

Recently, it has been shown that enzyme encapsulation inside metal–organic frameworks (MOFs) can increase enzyme activity and serve as protection from adverse environmental conditions. Little is understood about how the enzymes move into and are held inside the MOFs although it is believed that intermolecular forces between the MOF and the enzyme cause it to be held in place. If this process can be better understood, it can have dramatic implications on the cost-effectiveness and implementation of enzyme–MOF complexes. This is of specific importance in the medical sector for protein therapy and the industrial sector where enzyme use is expected to increase. Herein, we synthesized alcohol dehydrogenase (ADH) and PCN-333 to study encapsulation, stability, and enzyme activity to expand the knowledge of our field and offer a potential improvement to a synthetic route for biofuel synthesis. From this, we found a correlation between the concentration of a buffer and the loading of an enzyme, with surprising loading trends. We conclude that the buffer solution decreases interactions between the enzyme and MOF, supporting conventional theory and allowing it to penetrate deeper into

the structure causing higher enzyme loading while allowing for excellent stability over time at various pH values and temperatures and after multiple reactions. We also observe new trends such as a rebounding effect in loading and "out-of-bounds" reactions.

2.0.2 Introduction

Enzymes are highly conserved, fast, and efficient natural catalysts that increase the rate of reaction by lowering the required activation energy. Because of this, many industries have taken advantage of these catalytic masterpieces to increase reaction rates and efficiency.[16,50] A common method to further increase the reaction activity and longevity of enzymes has been through immobilization of enzymes.[51,52] Metal−organic frameworks (MOFs) have recently been shown to have a similar effect on enzymes through encapsulation and have become an increasingly popular area due to many advantages and applications they provide in a plethora of fields.[23,28,53,54] These porous structures are synthesized from a combination of various interchangeable organic linkers and metal ions, allowing their symmetry, shape, and size to be customized.[55–60] Under a suitable environment, the starting materials of a MOF combine to form highly stable and uniform crystalline structures. These can be tuned to withstand extreme temperature, pressure, and pH or can be synthesized so that they steadily dissociate in a target environment.[22,23,33,34,61–63] Furthermore, the linkers of a MOF can themselves be customized by the addition of functional groups. This characteristic interchangeability of components allows for endless design capabilities leading to an incredible amount of applications. Researchers have shown that MOFs can be utilized beneficially in applications such as gas sensing, gas storage,[27,64,65] catalytic mimics,[59,60,66–68] chemical separations,[69,70] cancer treatment,[71–73] and the encapsulation and immobilization of drugs/proteins.[28,29,34,41,56,62,74–85] Much of this is made

possible due to the porous nature of MOFs, which allows for the uptake, storage, and capture of materials like drugs, gases, harmful chemicals, and enzymes.[23,29,79,83,86,87] Recent developments in the encapsulation of enzymes have shown that they can be encapsulated inside the framework of a MOF with surprising benefits. Farha and co-workers have recently advanced the field by laying the foundation for MOF encapsulation, describing that enzymes can be encapsulated via de novo encapsulation (DNE) where the MOF forms around the enzyme, or by post synthetic encapsulation (PSE) where the MOF is formed and the enzymes later infiltrate the channel or cage-shaped pores by diffusion.[28,77,88–90] While encapsulated, the enzymes gain the ability to withstand harsh environments. These adverse conditions, like high temperature, high or low pH, and organic solvents, would naturally cause the enzyme to denature leading to potential permanent loss of function. Instead, the MOF housing protects and, in many cases, increases the activity of the protected enzyme.[28,49,56,77,78,80,84,89–92] In addition, Ma and co-workers recently presented a study on the effects of enzyme−MOF interactions and postulated that the reason enzymes are held in the interior of the MOF is due to intermolecular forces (IMFs) between the framework and the enzyme. These interactions cause the leashing of enzymes in the pores, making it difficult for them to escape.[32,37] Alcohol dehydrogenase (ADH) is a well-known enzyme found in humans that catalyzes the conversion of toxic levels of alcohols in cells to aldehydes.[93] The reverse reaction of this enzyme, however, can be utilized to convert aldehyde groups to alcohols and is used in the industry to synthesize chiral alcohols (Figure 1).[94] Because of the low specificity of the active site found in ADH, researchers have been able to use the enzyme in several industrial applications, including as a downstream effector in a chain of enzyme reactions that can convert lipids into alcohols, which

may be used as diesel-like biofuel.[93,94] Other works have already shown that the MOF encapsulation of lipase creates a functional complex that can catalyze the cleavage of ester bonds, which are found in lipids.[95] Thus, the combination of these encapsulated enzymes in solution may be used in future applications for biofuel synthesis from common lipid sources like waste oils from food production. While the applications of MOF-encapsulated enzymes are continuously being researched, the mechanisms involved in their interactions are not well understood. These interactions are more obvious in PSE, which has received less attention. This being most likely due to the popularity that comes from the ease of synthesis and the loading speed in DNE, with MOFs like zeolitic imidazole framework-8 (or ZIF8) when compared to the more rigorous organic synthesis required for MOFs suitable for PSE.[96] MOFs used in PSE often have the advantage of having larger pores but suffer from a more difficult, longer synthesis with the infiltration rates and loading of materials not readily available.[76,89,97] In this work, we focused on expanding the knowledge of our field by utilizing the cage-type MOF PCN-333(Fe) to perform a novel study on the factors affecting the encapsulation uptake, activity, and stability of ADH.[76,98] We chose this specific MOF because of its well-known stability and cage size in relation to the enzyme we wanted to study and because we wanted to observe the effects of PSE enzyme loading on a cage-type MOF as these have received less attention. Additionally, we chose to use this well-known enzyme as a model, utilizing its reverse reaction for alcohol synthesis and biofuel production, which, to the best of our knowledge, has never before been studied while being encapsulated in a MOF. The results of this study will benefit researchers who are interested in post synthetic encapsulation, factors affecting enzyme loading, stability,

and recyclability and may lead to enzymes like ADH having an increased role in future industrial applications for the synthesis of products like biofuel.

2.1.0 Experimental Section

2.1.1 Synthesis of ADH

The expression strain of AdhP was from the ASKA collection. The glycerol stock for AdhP was inoculated into 20 mL fresh LB medium and grown in 37 °C overnight. Then 20 mL overnight culture was transferred into 400 mL fresh LB medium with the supplement of 100 µg/mL chloramphenicol and cultured in shaker (250 rpm) at 37 °C until the absorbance of the media reached 0.6 to 0.8 at 600 nm. Then with an addition of 0.1 mM IPTG which was used to induce the expression of AdhP, cells were incubated at 30°C for another 5 hours. After harvested by centrifugation at 3,214 × g for 15 min at 4 °C, cells were resuspended in 12 mL lysis buffer [50 mM

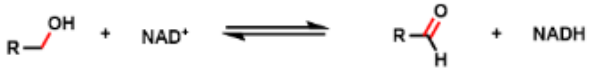

Figure 1 *Scheme depicting reaction of Alcohol Dehydrogenase (ADH)*

Tris (pH 8.0), 300 mM NaCl, 20 mM imidazole, and 1 mM DTT] supplemented with 1 µL nuclease, and then cells were lysed using ultrasonication, followed by centrifugation at 20,000 × g for 25 min at 4 °C. The supernatant was filtered through a 0.45 µm membrane and loaded onto a column containing 3 mL of Ni-NTA resin (Qiagen, Hilden, Germany) previously equilibrated with 20 mL lysis buffer. 20 mL washing buffer [50 mM Tris (pH 8.0), 300 mM NaCl, and 50 mM imidazole] was used to wash away those proteins without a His6-tag, while the AdhP protein with a His6-tag (AdhP) was bound to the column. 3 mL elution buffer [50 mM Tris (pH 8.0), 300 mM NaCl, and 150 mM imidazole] used to elute the His6-tagged AdhP from column.

2.1.2 Synthesis of PCN-333(Fe)

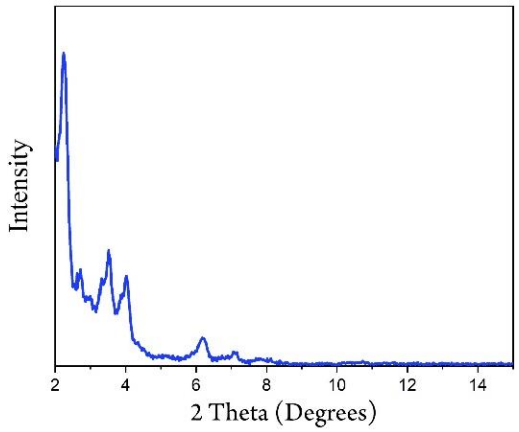

Figure 2 *Powder x-ray diffraction of synthesized PCN-333(Fe)*

The precursor 4,4′,4′′-s-triazine-2,4,6-triyl-tribenzoic acid (H_3TATB) and MOF PCN-333(Fe) were synthesized according to the method described in the work by Park et. al. 2015[35, 54]. In a 15 mL reaction vessel, we combined 60 mg H_3TATB, 60 mg anhydrous $FeCl_3$ (III), 0.6 mL TFA, and 10 mL DMF. The vessel was then sealed and placed in an oven at 135 °C for 12 hours. Brown precipitate formed and was collected by centrifugation. Product was washed several times each by DMF, acetone, and water with centrifugation after each step to collect. Water was then exchanged with acetone three times before activation in vacuum oven at 70 °C overnight. The product was then confirmed via X-ray diffraction (Figure 2).

2.1.3 Encapsulation of ADH in PCN-333(Fe)

An enzyme loading solution was created by combining ADH (0.5 mg/mL), Tris-HCl buffer at pH 7 (100 mM), PCN-333(Fe) (0.5 mg/mL), and water in a microcentrifuge tube (1.5 mL). This was allowed to sit for 7 days at 4 °C. The solution was agitated to resuspend the complex frequently several times a day by vortexed lightly. Other solutions were also prepared using the same procedure at 25 °C using 2 mM, 33 mM, and 100 mM Tris-HCl buffer and were stopped at 1, 3, and 7 days to determine percent loading. Amount of enzyme loaded was determined via the

Bradford assay method using Brilliant blue dye G and was corrected for the buffer concentration of each sample.[32,93] In another vial, enzyme was also tagged using AnaTag™ HiLyte Fluor™ 488 Microscale Protein Labeling Kit and allowed to infiltrate the MOF overnight before isolation and imaging using a confocal fluorescent microscope at 488nm to observe encapsulation (Figures 3b, 3c, 3e and 3f). A leaching test was also conducted in triplicate by taking 50 µL of enzyme loading solution, removing the supernatant, and washing the complex several times before returning the volume to 50 µL, vortexing, and allowing the solution with suspended ADH@PCN-333 to sit at 4 °C for 24 hours. The amount of enzyme in solution after this period was measured using the Bradford assay method.

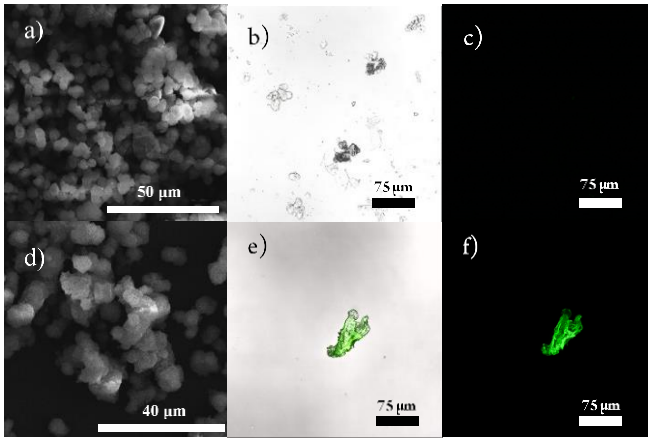

Figure 3 *a) SEM image of PCN-333. b & c) Confocal fluorescence microscopy images of PCN-333 under excitation of a 488 nm laser. d) SEM Image of ADH@PCN-333. e & f) Confocal florescent microscopy images of Alexaflor488 tagged ADH encapsulated in PCN-333 under excitation of a 488nm laser*

2.1.4 Activity measurement of ADH@PCN-333(Fe)

Activity of enzyme was determined by consumption of NADH at 340 nm using a Jasco V-770 UV accompanied with a Jasco ETCS-761 temperature controller with stirring capabilities. Reactions were conducted over a period of 10 min. at 37 °C with 3.75 µL of 200mM NADH, 3.23 µL Propionaldehyde, and 25mM Tris-HCl buffer at pH 7 with a final volume of 3 mL unless otherwise

stated. Reactions were monitored continuously with UV in a cuvette, stirring at 500 rpm. For each test, solutions containing buffer, water, and ADH@PCN-333 or controls were allowed to shake for 10 minutes before NADH and aldehyde were added to begin the reaction. All reactions were conducted under these conditions in triplicate and were compared to a standard reaction of free ADH that obtained the highest activity during the course of the particular test unless otherwise stated. The amount of enzyme in each control sample was dictated by the amount of loading of ADH into PCN-333. For reactions containing ADH@PCN-333, solutions containing the complex were agitated frequently by vortexing several times each day during the loading process to resuspend components. Then, after 7 days, three aliquots of 50 µL each of the loading solution were extracted each test. In order to isolate the complex and remove all excess ADH, the supernatant was removed after centrifugation in 4 cycles where the solution was allowed to sit for 10 min. before centrifugation at 1500 rpm for 10 minutes. Product was confirmed by GC-MS.

2.1.5 Effect of temperature on activity of ADH@PCN-333(Fe)

Activity of free ADH, ADH@PCN-333, and control solutions were monitored using consumption of NADH at 340 nm at 37 °C, 50 °C, 60 °C, 70 °C, and 80 °C. Results were compared to free ADH at 70 °C based their turnover frequency (TOF) after 5 minutes.

2.1.6 Effect of pH on activity of ADH@PCN-333(Fe)

Activity of ADH free enzyme, ADH@PCN-333, and control solutions were monitored using consumption of NADH at 340nm at a solution pH of 3, 5, 7, 9, or 11. Citrate buffer was used at pH 3 and 5, Tris-HCl at pH 7 and 9, and phosphate buffer at pH 11. All reaction solutions had concentrations of 25 mM buffer. Results were compared to free ADH at pH 7 based their turnover frequency (TOF) after 5 minutes.

2.1.7 Effect of solvent on activity of ADH@PCN-333(Fe)

Activity of ADH free enzyme, ADH@PCN-333, and control solutions were measured using consumption of NADH at 340 nm in solution containing 10% THF, 10% acetonitrile, or water. Samples were tested after 10 minutes and 24 hours in solution and were compared by TOF to ADH@PCN-333 in water after 10 minutes as the standard.

2.1.8 Stability of ADH@PCN-333(Fe)

Activity of ADH free enzyme, ADH@PCN-333, and control solutions were monitored using consumption of NADH at 340 nm after exposing stock solutions to room temperature and frequent agitation by vortexing to resuspend the samples several times each day for seven days. The room temperature sample solutions of free ADH and ADH@PCN-333 were then chilled overnight at 4 °C and the activities were again measured.

An additional test was conducted measuring loading and activity in relation to temperature and pH while receiving infrequent agitation by vortexing the samples twice every other day over the period of seven days. We named this portion of the Stability test the “duration test”. All samples were compared by TOF to a standard reaction of free ADH at pH 7 after 7 days at 4 °C receiving infrequent agitation.

2.1.9 Recyclability of ADH@PCN-333(Fe)

A 50 µL aliquot of ADH@PCN-333 stock solution containing 0.5mg/mL PCN-333 loaded with ADH at 23.7% was added into a 1.5 mL microcentrifuge tube and centrifuged. The supernatant was removed and replaced 3 times to remove any free ADH. After a final removal of supernatant, a 100 µL reaction mixture with 100 mM Tris-HCl was made by combining the complex in solution with water, buffer, 5 µL of 200 mM NADH, and 2.5 µL propionaldehyde. The reaction mixture was

briefly vortexed and allowed to react for 5 minutes on a shaker at 350 rpm and 37 °C. The tube was then centrifuged for 1 minute to collect the complex. 50 µL of supernatant was then extracted and diluted to 3mL, vortexed, and the absorbance at 340 nm was measured by UV and the consumption of NADH was determined. The leftover reaction mixture was then centrifuged for 5 minutes, and the supernatant was removed. The complex was then washed with water before the process was repeated.

2.1.10 GC-MS analysis

Activity of ADH and ADH@PCN-333 were also compared by GC-MS. Samples were placed in a 1.5 mL microcentrifuge tube with a final volume of 250 µL. The concentrations of components were 2 µL propionaldehyde, 10 mM pH 8 Tris-HCl buffer, and 118.8 µL of 200 mM NADH. The reaction was allowed to proceed for 30 minutes before extraction. The sample was kept at -20 °C until running on GC-MS. Before running the sample, it was allowed to thaw and was immediately injected into the GC-MS column.

2.1.11 Statistical analysis

Each experiment was performed in triplicate and values were given as means ± standard deviations. Differences between groups were compared by means of one-way ANOVA ($p < 0.05$). All statistical tests were performed using Excel 2016 (ver. 16051.12527.20278.0, Windows, USA)

2.2.0 Results and discussion

2.2.1 Encapsulation of ADH in PCN-333.

Recent publications have reported the successful encapsulation of several enzymes by both de novo synthesis of MOF around enzymes and PSE, which we utilize here.8 In this study, we chose to keep the concentration of MOF and enzyme in the stock-loading solution at a low

concentration (0.5 mg/mL) and a weight ratio of 1:1 to observe the factors affecting enzyme loading more closely. In addition, we chose an enzyme−MOF pair that had a small pore-to-enzyme volume ratio, with the largest pores of the cages in PCN-333 having diameters of 55 Å, while ADH's dimensions measured 52 × 37 × 30 Å. A representation of this encapsulation can be seen in Figure 4. While this appears to be a tight fit, the successful encapsulation inside this MOF of an enzyme with larger dimensions of 62 × 44 × 40 Å has already been reported.[99] Furthermore, enzymes have been shown to enter through pores of a much smaller size than that of their active conformation form of the enzyme, showing that they unravel, enter, and then reform into their active conformation.[28,37] Typically, the enzymes chosen for PSE are the same size or smaller than the entrance pore of the chosen MOF such as the case in a work by Farha and co-workers, where the researchers utilized the channel MOF NU-1003 with a pore size of 44 Å to encapsulate the enzyme organophosphorus acid anhydrolase (OPAA) with dimensions of 78 × 44 × 44 Å, allowing it to readily move inside.[90,93] Testing this variable allowed us to observe the rate at which an enzyme of such a size would enter the smaller outer pores found on the exterior of the cages in PCN-333. We were able to confirm the immobilization of ADH using a fluorescent tag after a loading period of 1 h and isolation using confocal fluorescent microscopy (Figure 3e,f) and compared it to plain PCN-333 under the same conditions (Figure 3b,c). This showed that there was an enzyme present, immobilized by PCN-333, with greater prevalence on the exterior of the particle, while its absence was observed in the bare PCN-333 sample. While this confirms the immobilization, at least on the surface, the later results obtained from the pH test made it clear that the enzymes were indeed encapsulated after the free ADH completely lost its activity below pH 7 while the encapsulated

form remained active. We then performed a loading test and found that as the concentration of the buffer in the loading solution increased from 10, 33, and 100 mM, the loading of ADH also increased (Figure 5a). There was a stark difference between the 10 and 100 mM samples with a maximum loading of 19 and 36%, respectively, at day 7 (Table S2). We believe this correlation arises due to the increase in interactions (i.e., hydrogen bonding, London dispersion forces, and dipole interactions) between the enzyme and buffer as opposed to interactions with the framework, which slows its movement through the framework's pore. The reverse of this effect should also be true for the leaching of enzyme where these forces would cause the enzyme to be gripped by the MOF leading to the low loss of enzyme into the solution. These results support the theory that the enzyme becomes immobilized in a MOF by IMFs, preventing its movement and release raised by Ma and coworkers.[37] There was an unexpected decrease in loading that can be seen with the loading of enzyme in the 10 mM buffer solution later in the experiment. Typically, the loading of enzyme appears to reach a peak and subsequently decreases but can return to the maximum or past the previous peak loading over time. This effect of a loading wave or rebound effect, where the amount of enzyme loaded reaches a maximum and then decreases, was observed in all samples given enough time but was more prominent in samples that received less agitation and lower loading over the course of the experiment (Figure 5 a & c and Tables S1 & S2). We believe the cause of this comes from an impasse created by the stoppage of enzymes filling the exterior pores of the MOF which become trapped in place, thus preventing the movement of more enzymes further into the MOF. These blocked enzymes then create a high concentration in the outer portion of the MOF leading to leaching back out into the solution by a concentration gradient. As the impeded

enzymes penetrate deeper into the MOF, the other enzymes are allowed to move into the vacated pores, thus leading to the higher uptake. Based on this theory and our results, we believe the higher loading of 100 mM buffer allows for fewer interactions between the enzymes and MOF, therefore allowing the enzymes to penetrate deeper into the MOF and leading to the observed higher loading percentage (Figure 5a,c). Additionally, when we compared the loadings of enzyme at room temperature to the same procedure at 4 °C, we noticed that the loading was significantly less at 24% compared to the former's 36% (Figure 5a). This is likely due to the decrease in the rate of folding and unfolding of the enzyme that must take place for the enzyme to move through the pores of the MOF. Alternatively, the increased rate of loading may also be attributed to denatured proteins created by the warmer temperature and vortexing, which may allow them to readily move into the pores. Another significant observation about the loading process was observed when we compared the loading of ADH at pH 7 versus pH 8. ADH is normally kept at pH 8 because it is more stable under this condition; however, we chose to keep the loading of enzymes used in each reaction at pH 7 during the 7-day loading period to amplify the protecting effect of the MOF. When we perform the loading test at pH 7 and 8, it was evident that the pH 8 solution showed a higher volatility in the results with a loading of 35% on day 3 compared to that of 20% by pH 7. Following that, when the rebound effect was observed at days 5 and 7, the loading dropped to 15% before going back up to 23%. This was compared to a decrease to 19% and a subsequent increase to 26% by the pH 7 sample. This result leads us to conclude that pH can be a major contributing factor to loading and can be manipulated to increase loading as well as to increase payload retention in MOFs by altering the amount of hydrogen bonding and other interactions that

occur. When leaching of enzyme from MOF was tested after the complex was washed and kept in solution for 24 h, only 1.5% of enzyme on average was found to be in solution. This shows that the complex has good enzyme retention. We believe this value could have further been reduced with more solvent exchange cycles and therefore the extraction of buffer molecules from inside the framework. This is drawn from our theory that as the excess buffer is removed by washing and exchange, there are increasing interactions between the enzyme and surrounding MOF, thus allowing it to be better leashed inside the pore. Several factors to consider when trying to increase the enzyme loading would be to use a MOF with a large pore size comparable to the chosen enzyme, use higher concentrations of the buffer, and decrease the particle size of MOFs used. Each of these avenues would either decrease the interactions between the enzyme and the MOF or increase the surface area and thus available pores of the MOFs used. However, it should be stated that because these interactions are heavily dependent on proximity, with the larger pore size, one should expect higher leaching, which would cause the recyclability to suffer.

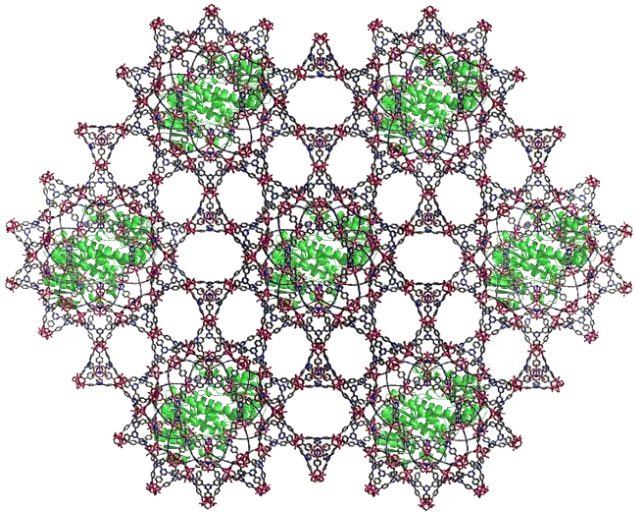

Figure 4 *Representation of optimal loading of ADH enzyme inside PCN-333's largest cages*

2.2.2 Stability of ADH@PCN-333 over time

To keep enzymes at their optimal state and prevent them from deteriorating, they are usually kept in buffer at a specific pH and at 4 °C or lower. By testing the stability of the enzyme, in both the encapsulated and free forms, to the best of our knowledge, we present the most in-depth study to date on the longevity and efficient loading of enzyme into a MOF. In this work, we found that when kept at room temperature the encapsulated form of ADH suffered a loss of 20% in activity compared to our control group of free ADH kept at 4 °C after a reaction time of 5 min. In comparison, the free ADH kept at room temperature lost all its activity (Figure 5a). Alternatively, the enzyme encapsulated at 4 °C over the same period lost very little activity (5%). The small loss of activity seen from the ADH@PCN-333 at room temperature may be due to a decrease in the amount of enzyme loaded inside the MOF, but we believe it is due mostly to the denaturing or partial unfolding of enzyme located on the exterior of the MOF in unclosed pores or those that have only incompletely moved into the pores and are caught in an inactive state. Interestingly, we found that after the encapsulated ADH was kept at room temperature for a week and was subsequently allowed to stay at 4 °C overnight, some of this lost activity was recouped. The activity increased to 90%, a 15% increase. We believe that this retrieval of lost activity comes from enzymes leashed in unclosed pores or the exterior of the MOF that have partially unfolded into a nonactive form and that the decrease in temperature leads to refolding to their active state.

In addition to the temperature comparison in the stability test in Figure 5a, we also measured the activity of the enzyme–MOF complex over a week at different conditions to determine the

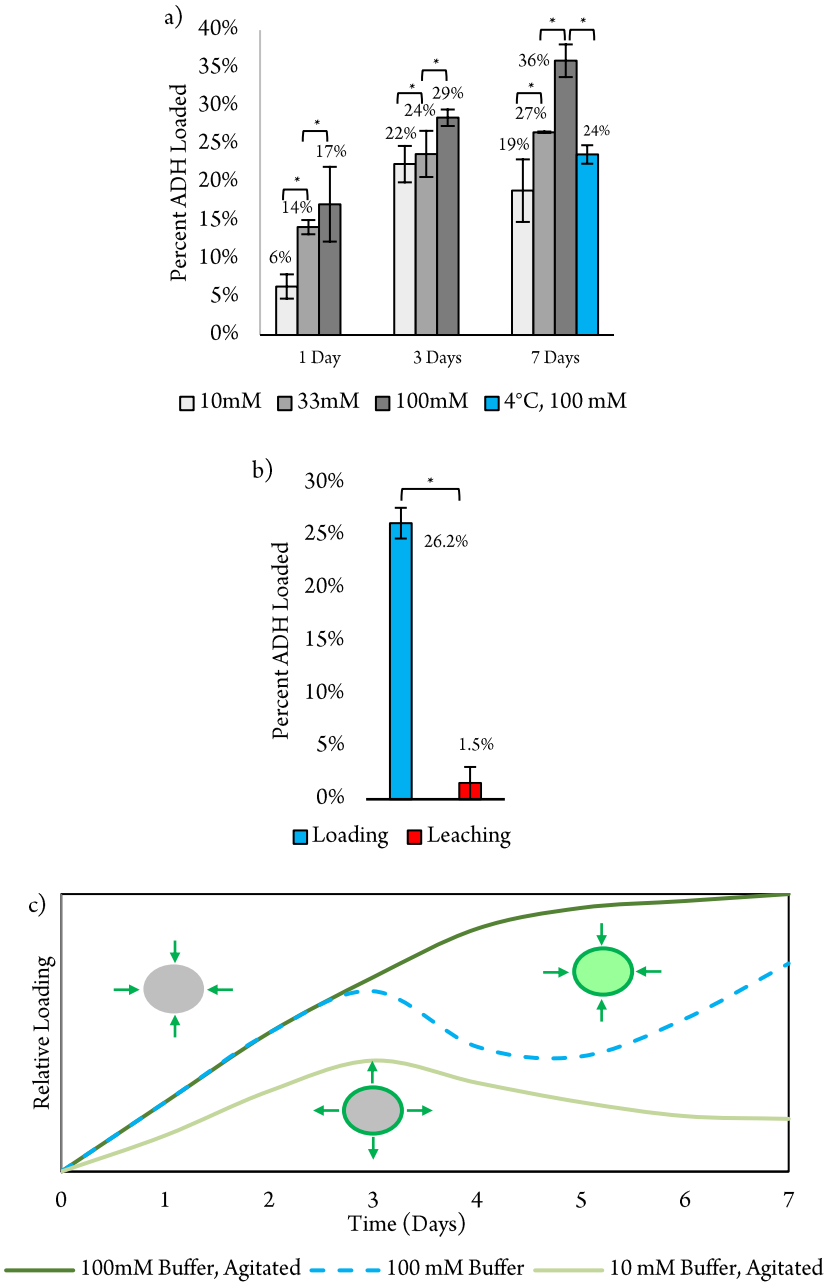

Figure 5 *Plot depicting the room-temperature loading of ADH in PCN-333 at an increasing buffer concentration over time with frequent agitation for resuspension. (b) Loading of ADH@PCN-333 at 4 °C after 7 days compared to the leaching of ADH from MOF after 24 h in solution. * Indicates significant between-group differences (P < 0.05). Error bars indicate ± standard deviation. (c) Graph depicting differences in loading trends observed and the rebound effect observed between samples that were vortexed multiple times a day (agitated) or twice every other day with either 10 mM or 100 mM buffer.*

stability of the loaded enzyme over time in relation to its enzyme loading (Figure 5b, c). When we compared the overall consumption of NADH per sample at day 0, our results showed the pH 7 at 4 °C sample yielding 91%, the room temperature sample yielding 101%, and the pH 8 of 4 °C sample yielding 95% in relation to that of free ADH (Figure 5b). On day 7, these results became 103, 93, and 88%, respectively (Figure 5b). Here, we found that there was little variance in our results between days 0 and 7, with the pH 7 at 4 °C sample consistently outperformed the others during the test after day 0. We had predicted that the activity of enzymes in solution would decrease over time in the suboptimal condition of pH 7 compared to that of pH 8 before being loaded into the complex. However, the results showed that this had little to no effect on yield.

When we compared the consumption of NADH to enzyme loading, we found that there was an inverse correlation. In the room-temperature sample, as the loading decreased from days 1, 3, and 7, the activity per enzyme increased from 102 to 111 and 127%, respectively, in relation to the free ADH standard. (Figure 5c and Table S1). We believe that this is due to the further isolation of individual enzymes arising from the increased movement allowed in relation to temperature, giving the enzymes the ability to further penetrate the MOF. As the loading increases, it follows that the possible loading of two or more enzymes moving into the same cage increases. This infiltration and competition of space likely lead to the inactivity of both enzymes. This is the reason for Figure 3 depicting the “optimal” loading of ADH. In practice, we consistently observed changes in loading over time, so it is not likely that this optimal condition is the final state. However, this desired ideal state of the enzymes in MOF may occur given enough time to diffuse throughout the framework.

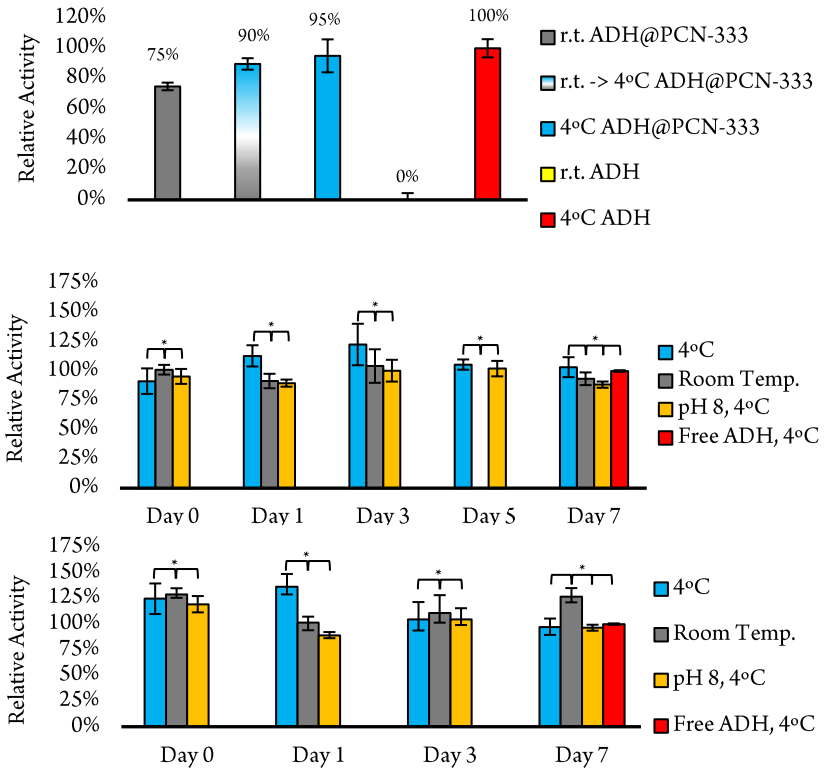

Figure 6 *a) Plot of activity during the stability test, depicting results comparing the turnover number of ADH@PCN-333 and free ADH samples at a reaction time of 5 min after 1 week at room temperature or at 4 °C while receiving frequent agitation. b) Graph of the duration test presenting activity based on the consumption of NADH at 5 min of samples over a period of 1 week as loading proceeds. c) Comparison of the relative activity in the duration test of samples at 5 min based on the turnover number over a period of 1 week as loading proceeds. *Indicates significant between-group differences (P < 0.05). Error bars indicate ± standard deviation.*

One major difference in the method of the loading over time test (Table S1) versus the temperature and buffer test (Figure 4a and Table S2) is that the latter samples were vortexed to resuspend the solution multiple times a day. In the former test, the samples were only resuspended by vortex two times every other day. When we compare the 4 °C samples with high agitation, we see very little difference, with the sample receiving low agitation having a loading of 26% after 7 days compared to the high agitation yielding 24%. This is significantly different in the room-temperature samples, where the low agitation yielded 19% loading after 7 days compared to 36% by the highly agitated sample. In terms of activity, in relation to free

ADH at pH 7 and 37 °C, the higher agitated samples produced a yield of 80%, while the samples that received lower agitation retained most of their activity, achieving a yield of 97% after 7 days. From these results, it is evident that this disruption may have caused the loading in the temperature and buffer test to be higher at the cost of enzyme activity, while in the duration test, the enzymatic activity was retained and was comparable to that of the free enzyme.

2.2.3 Effect of pH on ADH@PCN-333 activity

Because the activity of ADH is reported and well known, the choice of pH values to study were chosen to observe the trend of activity as pH changed and not to reproduce known results. As expected, we observed little to no activity at pH 9 and 11, with both forms of ADH not achieving any activity over 10% in relation to free ADH's highest activity (100%) at pH 7 (Figure 6a). Additionally, we anticipated that the activity of the encapsulated enzyme would increase as the pH decreased below pH 7. Instead, we observed the activity of the encapsulated enzyme to drop at pH 5 to 19% and then recover much of its lost activity when the solution was set to pH 3 with a yield of 92%. In contrast, the free enzyme produced no activity under either of these acidic conditions. Aside from this result, the behavior of the enzyme appears to follow the activity trend of other reported experiments, where the maximal activity in the reverse direction was near pH 7.[100] At this condition, the free form of ADH achieved a yield of 0.35 U/min at 5 min and the encapsulated form achieved an 80% yield in relation to tha t. The lower activity of the encapsulated enzyme was attributed to the previously mentioned agitation of the reaction mixture and room temperature loading, from which we concluded that either some of the enzymes became inactive before moving into the MOF and did not return to their active state after incorporation or there was an increase of interactions of enzymes in the same

pore causing both enzymes to fail to return to their active state. This is further supported by the data represented in our stability test where the samples under the same conditions were not agitated frequently and showed relatively the same activity. Thus, decreasing the agitation of samples can lead to a larger portion of active versus nonactive loaded enzymes. The increased activity at pH 3 supports the theory that the isolation of enzymes and the surrounding MOF framework can help increase the reaction rate and prevent the enzyme from deteriorating or unfolding at adverse pH. It appears that the manipulation of pH, possibly along with other

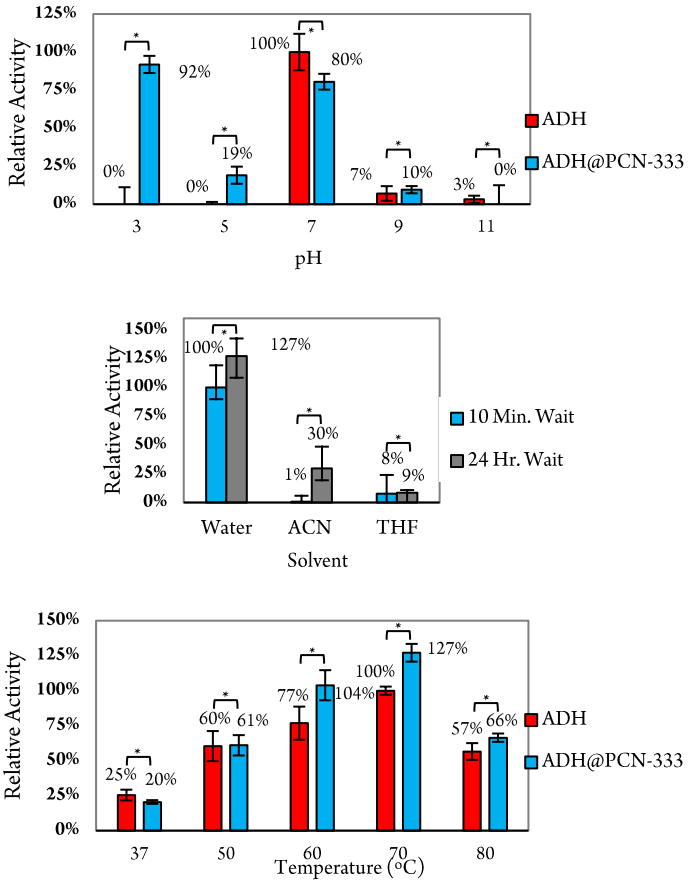

Figure 7 *a) Comparison of relative activity based on turnover number of free ADH and ADH@PCN-333 after resting in various pH before reacting at 37°C for 5 minutes. b) Comparison of turnover number of ADH@PCN-333 after resting in 10% organic solvent for 10 min. or 24 hours before reacting at 37°C for 10 min. c) Comparison of relative activity based on turnover number of ADH and ADH@PCN-333 after resting at various temperatures before reacting at those temperatures for 5 minutes. * Indicates significant between-group differences (P < 0.05). Error bars indicate ±*

conditions, has the potential to lead to the production of products at a possibly higher rate than the native enzyme under conditions that would be favorable to the reaction but not the fragile enzyme. Our lab has taken to calling this an “out-of-bounds” reaction because the reaction occurs outside of the boundaries or conditions natural to the enzyme.

2.2.4 Effect of solvent on the activity of ADH@PCN-333

ADH@PCN-333 displayed its best activity after soaking in water for 24 h, showing a 127% yield relative to its yield after the normal 10 min wait condition (the standard for this test). This increase in activity can be attributed to the smaller buffer concentration located in or near the MOF. This is because in the other tests, the solution containing the MOF complex is exchanged a minimum of three times before the reaction takes place and this may not be done over enough time or enough iterations to fully remove the high concentration of buffer from within the MOF. This would lead to a slower reaction as the concentration of the buffer was found to be indirectly correlated to the activity of the enzyme. Thus, this 24 h period appears to allow for the excess buffer to be pulled out of the MOF complex causing faster reactivity of the housed enzymes. While some of the enzymes would escape and be free in solution, we believe these enzymes would not significantly contribute to any improved reactivity based on our tests in Figure 5. These show relatively the same activity between free and encapsulated ADH. The activity of the complex was significantly diminished when tested in a solution with acetonitrile. However, this same increasing trend in activity was observed with a yield of 30% after the 24 h pause and 1% yield after the 10 min wait. Alternatively, we discovered that there was a decrease in activity of the complex after the incorporation of THF, with the yield achieved after 10 min and 24 h being 8 and 9%, respectively. This leads us to believe that the polarity and the

nature of the solvent are important factors for ADH activity, and as the polarity decreases, so does the activity ADH. This result shows that while some enzymes continue to function with the addition of organic solvents, it is not a steadfast rule and may be an important factor to consider.

2.2.5 Effect of temperature on ADH@PCN-333 activity

We found that there was a direct relationship between temperature and the activity of the enzyme, both in its free and encapsulated states (Figure 6c). The encapsulated enzyme did not outperform the free enzyme at the physiological temperature, where it had a 20% yield at 5 min compared to 25% by the free form. Its activity was comparable at 50 °C, with the average of the encapsulated form being 61% compared to 60% by the free form. Starting at 60 °C, the encapsulated enzyme finally significantly outperformed the free enzyme with an activity of 104% compared to that of 77% by the free enzyme. The encapsulated ADH continued to outperform at 70 °C, where we reported the maximal activity for both samples. At this temperature, the encapsulated form achieved a yield of 127% compared to the free form's yield of 100% (the standard for this test). Here, the activity came to 1.4 U/min for the free enzyme, while we observed a turnover of 1.8 U/min for the encapsulated form. At 80 °C, the activity of ADH decreased for both the encapsulated ADH and the free form, with yields of 66 and 57%, respectively. We originally anticipated the yield being lower as the temperature increased due to denaturing. However, because the free enzyme also functions well under these conditions and follows the same trend as the temperature increases, we concluded that the increased activity of the encapsulated enzyme owed mostly to its ability to isolate the enzyme inside the cages of the MOF.

2.2.6 Recyclability of ADH@PCN-333

The ability to reuse enzymes in catalysis is a major contributing factor when calculating the cost efficiency of a process and is one of the hallmarks of MOF-encapsulated enzymes. Previous works have reported good recyclability for ADH when immobilized but a loss of activity after just a few cycles.[91,101] In contrast, our results showed that after 10 reaction cycles the encapsulated enzyme showed no decrease in activity (Figure 7a). We believe that this outstanding performance can be attributed to the ability of the cage-type MOF to better leash the enzymes inside its pores and the complimentary size of the MOF cage to that of the enzyme, as previously mentioned. This relative volume of the MOF cage and enzyme, which gives the two a hand-in glove fit, appears to confer better isolation of the encapsulated enzyme, and prevents the enzyme from readily leaching into the solution.

2.2.7 Confirmation of the product

To confirm the presence and compare the yield of 1-propanol product, GC−MS was conducted on samples of free ADH and ADH@PCN-333 under the best conditions observed (Figures S1 and S2). The free enzyme produced a turnover number of 3.87 U/min, while ADH@PCN-333 outperformed it with a turnover number of 4.64 U/min, thus yielding a 20% increase in activity (Figure 7b). This corresponds to the increase in activity that we observed in the duration test (Figure 5c). The increased activity of the enzyme overall compared to that of our other tests can be attributed to the decrease in buffer concentration. In our preliminary tests, we observed that there was a strong indirect correlation between the concentration of the buffer and the activity of the enzyme. Because of this, we had to choose a buffer concentration that would allow us to observe the differences in activity between samples but would not overly hinder the

reaction rate. We found that 25 mM of buffer was a “goldilocks” value, where the reaction did not occur too fast and allowed us to easily see the differences between samples. In this test, because we were not hindered by the use of the UV, to monitor the consumption of NADH, we removed this requirement and reduced the buffer concentration to 10 mM at pH 8.

2.3.0 Conclusions from experiment

In this paper, we perform a study on the encapsulation, stability, and activity of alcohol dehydrogenase in the cage-type MOF PCN-333(Fe) to better understand the loading process and provide a reusable complex for green synthesis of a model alcohol from aldehyde. Here, we show that the increased buffer concentration and thus the increased interactions between the buffer and enzyme as opposed to those of the enzyme and MOF can lead to higher loading of enzymes via post-synthetic encapsulation. Based on this result, we believe that the leaching from MOFs can also be limited by the use of a lower concentration of buffer, when possible, in storage. We also present results that further support the theory that MOFs can be used to increase reaction rates and the effective life span of enzymes all while under the protection of the surrounding MOF by encapsulation. Additionally, we show that while high agitation increased loading and higher loading yields more product, this also leads to lower activity per enzyme. This leads us to conclude that with higher loading, some enzymes infiltrate the already occupied pores and interact with other enzymes leading to fewer isolated and active enzymes. These interactions and higher concentrations inside the MOF lead to a rebounding effect in loading. This we were able to minimize with lower agitation and higher buffer concentration with which we postulate leads to greater penetration of enzymes into the interior of the MOF and higher loading. We also observed that while the enzyme activity can be increased under

normal conditions, reactions can also occur and can possibly be further improved in out-of-bounds reactions where conditions are augmented to create a beneficial environment for a reaction to occur at conditions that would have otherwise caused the free enzyme to be denatured. The excellent recyclability, stability, and increased loading for MOF-encapsulated enzymes presented in this work make them a suitable tool for the increased activity and longevity of enzymes in industrial applications. In addition, the method for increased loading can be utilized in the encapsulation of both enzymes and drugs for medical uses in MOFs to increase the payload. This area of study is still relatively new and continuously produces new and exciting applications. The implications of this and related works have the potential to dramatically affect markets in the near future as new developments are continually being made. By reducing the need for fresh enzymes while increasing their stability and activity, enzyme encapsulation in MOFs is proving to be an effective tool for consideration that can simultaneously cut the cost and increase product yield.

2.4.0 References

1) Singh, R.; Kumar, M.; Mittal, A.; Mehta, P. K. Microbial Enzymes: Industrial Progress in 21st Century. 3 Biotech 2016, 6 (2), 174. https://doi.org/10.1007/s13205-016-0485-8.

(2) Chapman, J.; Ismail, A. E.; Dinu, C. Z. Industrial Applications of Enzymes: Recent Advances, Techniques, and Outlooks. Catalysts 2018, 8 (6), 238. https://doi.org/10.3390/catal8060238.

(3) Rubenwolf, S.; Kerzenmacher, S.; Zengerle, R.; von Stetten, F. Strategies to Extend the Lifetime of Bioelectrochemical Enzyme Electrodes for Biosensing and Biofuel Cell Applications. Appl. Microbiol. Biotechnol. 2011, 89 (5), 1315–1322. https://doi.org/10.1007/s00253-010-3073-6.

(4) Zhang, Y.; Ge, J.; Liu, Z. Enhanced Activity of Immobilized or Chemically Modified Enzymes. ACS Catal. 2015, 5 (8), 4503–4513. https://doi.org/10.1021/acscatal.5b00996.

(5) Furukawa, H.; Cordova, K. E.; O'Keeffe, M.; Yaghi, O. M. The Chemistry and Applications of Metal-Organic Frameworks. Science 2013, 341 (6149), 1230444. https://doi.org/10.1126/science.1230444.

(6) Liu, R.; Yu, T.; Shi, Z.; Wang, Z. The Preparation of Metal–Organic Frameworks and Their Biomedical Application. Int. J. Nanomedicine 2016, 11, 1187–1200. https://doi.org/10.2147/IJN.S100877.

(7) Wang, P.-L.; Xie, L.-H.; Joseph, E. A.; Li, J.-R.; Su, X.-O.; Zhou, H.-C. Metal–Organic Frameworks for Food Safety. Chem. Rev. 2019, 119 (18), 10638–10690. https://doi.org/10.1021/acs.chemrev.9b00257.

(8) Majewski, M. B.; Howarth, A. J.; Li, P.; Wasielewski, M. R.; Hupp, J. T.; Farha, O. K. Enzyme Encapsulation in Metal–Organic Frameworks for Applications in Catalysis. CrystEngComm 2017, 19 (29), 4082–4091. https://doi.org/10.1039/C7CE00022G.

(9) Iv, J. J. P.; Perman, J. A.; Zaworotko, M. J. Design and Synthesis of Metal–Organic Frameworks Using Metal–Organic Polyhedra as Supermolecular Building Blocks. Chem. Soc. Rev. 2009, 38 (5), 1400–1417. https://doi.org/10.1039/B807086P.

(10) Lian, X.; Fang, Y.; Joseph, E.; Wang, Q.; Li, J.; Banerjee, S.; Lollar, C.; Wang, X.; Zhou, H.-C. Enzyme–MOF (Metal–Organic Framework) Composites. Chem. Soc. Rev. 2017, 46 (11), 3386–3401. https://doi.org/10.1039/C7CS00058H.

(11) Tranchemontagne, D. J.; Mendoza-Cortés, J. L.; O'Keeffe, M.; Yaghi, O. M. Secondary Building Units, Nets and Bonding in the Chemistry of Metal–Organic Frameworks. Chem. Soc. Rev. 2009, 38 (5), 1257–1283. https://doi.org/10.1039/B817735J.

(12) Kalmutzki, M. J.; Hanikel, N.; Yaghi, O. M. Secondary Building Units as the Turning Point in the Development of the Reticular Chemistry of MOFs. Sci. Adv. 4 (10), eaat9180. https://doi.org/10.1126/sciadv.aat9180.

(13) Beyzavi, H.; Klet, R. C.; Tussupbayev, S.; Borycz, J.; Vermeulen, N. A.; Cramer, C. J.; Stoddart, J. F.; Hupp, J. T.; Farha, O. K. A Hafnium-Based Metal–Organic Framework as an Efficient and Multifunctional Catalyst for Facile CO2 Fixation and Regioselective and Enantioretentive Epoxide Activation. J. Am. Chem. Soc. 2014, 136 (45), 15861–15864. https://doi.org/10.1021/ja508626n.

(14) Beyzavi, H.; Vermeulen, N. A.; Howarth, A. J.; Tussupbayev, S.; League, A. B.; Schweitzer, N. M.; Gallagher, J. R.; Platero-Prats, A. E.; Hafezi, N.; Sarjeant, A. A.; Miller, J. T.; Chapman, K. W.; Stoddart, J. F.; Cramer, C. J.; Hupp, J. T.; Farha, O. K. A Hafnium-Based Metal–Organic Framework as a Nature-Inspired Tandem Reaction Catalyst. J. Am. Chem. Soc. 2015, 137 (42), 13624–13631. https://doi.org/10.1021/jacs.5b08440.

(15) Ding, M.; Cai, X.; Jiang, H.-L. Improving MOF Stability: Approaches and Applications. Chem. Sci. 2019, 10 (44), 10209–10230. https://doi.org/10.1039/C9SC03916C.

(16) Luzuriaga, M. A.; Welch, R. P.; Dharmarwardana, M.; Benjamin, C. E.; Li, S.; Shahrivarkevishahi, A.; Popal, S.; Tuong, L. H.; Creswell, C. T.; Gassensmith, J. J. Enhanced Stability and Controlled Delivery of MOF-Encapsulated Vaccines and Their Immunogenic Response In Vivo. ACS Appl. Mater. Interfaces 2019, 11 (10), 9740–9746. https://doi.org/10.1021/acsami.8b20504.

(17) Chen, T.-T.; Yi, J.-T.; Zhao, Y.-Y.; Chu, X. Biomineralized Metal–Organic Framework Nanoparticles Enable Intracellular Delivery and Endo-Lysosomal Release of Native Active Proteins. J. Am. Chem. Soc. 2018, 140 (31), 9912–9920. https://doi.org/10.1021/jacs.8b04457.

(18) Long, J. R.; Yaghi, O. M. The Pervasive Chemistry of Metal–Organic Frameworks. Chem. Soc. Rev. 2009, 38 (5), 1213–1214. https://doi.org/10.1039/B903811F.

(19) Lei, B.; Wang, M.; Jiang, Z.; Qi, W.; Su, R.; He, Z. Constructing Redox-Responsive Metal–Organic Framework Nanocarriers for Anticancer Drug Delivery. ACS Appl. Mater. Interfaces 2018, 10 (19), 16698–16706. https://doi.org/10.1021/acsami.7b19693.

(20) Howarth, A. J.; Liu, Y.; Li, P.; Li, Z.; Wang, T. C.; Hupp, J. T.; Farha, O. K. Chemical, Thermal and Mechanical Stabilities of Metal–Organic Frameworks. Nat. Rev. Mater. 2016, 1 (3), 1–15. https://doi.org/10.1038/natrevmats.2015.18.

(21) Rosi, N. L.; Eckert, J.; Eddaoudi, M.; Vodak, D. T.; Kim, J.; O'Keeffe, M.; Yaghi, O. M. Hydrogen Storage in Microporous Metal-Organic Frameworks. Science 2003, 300 (5622), 1127–1129. https://doi.org/10.1126/science.1083440.

(22) Gulcay, E.; Erucar, I. Biocompatible MOFs for Storage and Separation of O2: A Molecular Simulation Study. Ind. Eng. Chem. Res. 2019, 58 (8), 3225–3237. https://doi.org/10.1021/acs.iecr.8b04084.

(23) Gadipelli, S.; Guo, Z. Postsynthesis Annealing of MOF-5 Remarkably Enhances the Framework Structural Stability and CO2 Uptake. Chem. Mater. 2014, 26 (22), 6333–6338. https://doi.org/10.1021/cm502399q.

(24) Jin, C.; Zhang, S.; Zhang, Z.; Chen, Y. Mimic Carbonic Anhydrase Using Metal–Organic Frameworks for CO2 Capture and Conversion. Inorg. Chem. 2018, 57 (4), 2169–2174. https://doi.org/10.1021/acs.inorgchem.7b03021.

(25) Hou, C.; Wang, Y.; Ding, Q.; Jiang, L.; Li, M.; Zhu, W.; Pan, D.; Zhu, H.; Liu, M. Facile Synthesis of Enzyme-Embedded Magnetic Metal–Organic Frameworks as a Reusable Mimic Multi-Enzyme System: Mimetic Peroxidase Properties and Colorimetric Sensor. Nanoscale 2015, 7 (44), 18770–18779. https://doi.org/10.1039/C5NR04994F.

(26) Zheng, H.-Q.; Liu, C.-Y.; Zeng, X.-Y.; Chen, J.; Lü, J.; Lin, R.-G.; Cao, R.; Lin, Z.-J.; Su, J.-W. MOF-808: A Metal–Organic Framework with Intrinsic Peroxidase-Like Catalytic Activity at Neutral PH for Colorimetric Biosensing. Inorg. Chem. 2018, 57 (15), 9096–9104. https://doi.org/10.1021/acs.inorgchem.8b01097.

(27) Adatoz, E.; Avci, A. K.; Keskin, S. Opportunities and Challenges of MOF-Based Membranes in Gas Separations. Sep. Purif. Technol. 2015, 152, 207–237. https://doi.org/10.1016/j.seppur.2015.08.020.

(28) Li, J.-R.; Kuppler, R. J.; Zhou, H.-C. Selective Gas Adsorption and Separation in Metal–Organic Frameworks. Chem. Soc. Rev. 2009, 38 (5), 1477–1504. https://doi.org/10.1039/B802426J.

(29) Kim, K.; Lee, S.; Jin, E.; Palanikumar, L.; Lee, J. H.; Kim, J. C.; Nam, J. S.; Jana, B.; Kwon, T.-H.; Kwak, S. K.; Choe, W.; Ryu, J.-H. MOF × Biopolymer: Collaborative Combination of Metal–Organic Framework and Biopolymer for Advanced Anticancer Therapy. ACS Appl. Mater. Interfaces 2019, 11 (31), 27512–27520. https://doi.org/10.1021/acsami.9b05736.

(30) Rowe, M. D.; Thamm, D. H.; Kraft, S. L.; Boyes, S. G. Polymer-Modified Gadolinium Metal-Organic Framework Nanoparticles Used as Multifunctional Nanomedicines for the Targeted Imaging and Treatment of Cancer. Biomacromolecules 2009, 10 (4), 983–993. https://doi.org/10.1021/bm900043e.

(31) Sakamaki, Y.; Ozdemir, J.; Heidrick, Z.; Watson, O.; Shahsavari, H. R.; Fereidoonnezhad, M.; Khosropour, A. R.; Beyzavi, M. H. Metal–Organic Frameworks and Covalent Organic Frameworks as Platforms for Photodynamic Therapy. Comments Inorg. Chem. 2018, 38 (6), 238–293. https://doi.org/10.1080/02603594.2018.1542597.

(32) Liang, S.; Wu, X.-L.; Xiong, J.; Zong, M.-H.; Lou, W.-Y. Metal-Organic Frameworks as Novel Matrices for Efficient Enzyme Immobilization: An Update Review. Coord. Chem. Rev. 2020, 406, 213149. https://doi.org/10.1016/j.ccr.2019.213149.

(33) Abazari, R.; Mahjoub, A. R.; Ataei, F.; Morsali, A.; Carpenter-Warren, C. L.; Mehdizadeh, K.; Slawin, A. M. Z. Chitosan Immobilization on Bio-MOF Nanostructures: A Biocompatible PH-Responsive Nanocarrier for Doxorubicin Release on MCF-7 Cell Lines of Human Breast Cancer. Inorg. Chem. 2018, 57 (21), 13364–13379. https://doi.org/10.1021/acs.inorgchem.8b01955.

(34) Zhang, H.; Jiang, W.; Liu, R.; Zhang, J.; Zhang, D.; Li, Z.; Luan, Y. Rational Design of Metal Organic Framework Nanocarrier-Based Codelivery System of Doxorubicin Hydrochloride/Verapamil Hydrochloride for Overcoming Multidrug Resistance with Efficient Targeted Cancer Therapy. ACS Appl. Mater. Interfaces 2017, 9 (23), 19687–19697. https://doi.org/10.1021/acsami.7b05142.

(35) Leng, X.; Dong, X.; Wang, W.; Sai, N.; Yang, C.; You, L.; Huang, H.; Yin, X.; Ni, J. Biocompatible Fe-Based Micropore Metal-Organic Frameworks as Sustained-Release Anticancer Drug Carriers. Molecules 2018, 23 (10), 2490. https://doi.org/10.3390/molecules23102490.

(36) Feng, D.; Liu, T.-F.; Su, J.; Bosch, M.; Wei, Z.; Wan, W.; Yuan, D.; Chen, Y.-P.; Wang, X.; Wang, K.; Lian, X.; Gu, Z.-Y.; Park, J.; Zou, X.; Zhou, H.-C. Stable Metal-Organic Frameworks

Containing Single-Molecule Traps for Enzyme Encapsulation. Nat. Commun. 2015, 6 (1), 5979. https://doi.org/10.1038/ncomms6979.

(37) Li, P.; Moon, S.-Y.; Guelta, M. A.; Harvey, S. P.; Hupp, J. T.; Farha, O. K. Encapsulation of a Nerve Agent Detoxifying Enzyme by a Mesoporous Zirconium Metal–Organic Framework Engenders Thermal and Long-Term Stability. J. Am. Chem. Soc. 2016, 138 (26), 8052–8055. https://doi.org/10.1021/jacs.6b03673.

(38) Nadar, S. S.; Rathod, V. K. Magnetic-Metal Organic Framework (Magnetic-MOF): A Novel Platform for Enzyme Immobilization and Nanozyme Applications. Int. J. Biol. Macromol. 2018, 120, 2293–2302. https://doi.org/10.1016/j.ijbiomac.2018.08.126.

(39) Hartlieb, K. J.; Ferris, D. P.; Holcroft, J. M.; Kandela, I.; Stern, C. L.; Nassar, M. S.; Botros, Y. Y.; Stoddart, J. F. Encapsulation of Ibuprofen in CD-MOF and Related Bioavailability Studies. Mol. Pharm. 2017, 14 (5), 1831–1839. https://doi.org/10.1021/acs.molpharmaceut.7b00168.

(40) Lyu, F.; Zhang, Y.; Zare, R. N.; Ge, J.; Liu, Z. One-Pot Synthesis of Protein-Embedded Metal–Organic Frameworks with Enhanced Biological Activities. Nano Lett. 2014, 14 (10), 5761–5765. https://doi.org/10.1021/nl5026419.

(41) Wu, X.; Ge, J.; Yang, C.; Hou, M.; Liu, Z. Facile Synthesis of Multiple Enzyme-Containing Metal–Organic Frameworks in a Biomolecule-Friendly Environment. Chem. Commun. 2015, 51 (69), 13408–13411. https://doi.org/10.1039/C5CC05136C.

(42) Zhang, C.; Wang, X.; Hou, M.; Li, X.; Wu, X.; Ge, J. Immobilization on Metal–Organic Framework Engenders High Sensitivity for Enzymatic Electrochemical Detection. ACS Appl. Mater. Interfaces 2017, 9 (16), 13831–13836. https://doi.org/10.1021/acsami.7b02803.

(43) Wu, X.; Yue, H.; Zhang, Y.; Gao, X.; Li, X.; Wang, L.; Cao, Y.; Hou, M.; An, H.; Zhang, L.; Li, S.; Ma, J.; Lin, H.; Fu, Y.; Gu, H.; Lou, W.; Wei, W.; Zare, R. N.; Ge, J. Packaging and Delivering Enzymes by Amorphous Metal-Organic Frameworks. Nat. Commun. 2019, 10 (1), 5165. https://doi.org/10.1038/s41467-019-13153-x.

(44) Hu, C.; Bai, Y.; Hou, M.; Wang, Y.; Wang, L.; Cao, X.; Chan, C.-W.; Sun, H.; Li, W.; Ge, J.; Ren, K. Defect-Induced Activity Enhancement of Enzyme-Encapsulated Metal-Organic Frameworks Revealed in Microfluidic Gradient Mixing Synthesis. Sci. Adv. 6 (5), eaax5785. https://doi.org/10.1126/sciadv.aax5785.

(45) Chen, Y.; Li, P.; Zhou, J.; Buru, C. T.; Đorđević, L.; Li, P.; Zhang, X.; Cetin, M. M.; Stoddart, J. F.; Stupp, S. I.; Wasielewski, M. R.; Farha, O. K. Integration of Enzymes and Photosensitizers in a Hierarchical Mesoporous Metal–Organic Framework for Light-Driven CO2 Reduction. J. Am. Chem. Soc. 2020, 142 (4), 1768–1773. https://doi.org/10.1021/jacs.9b12828.

(46) Sun, Q.; Fu, C.-W.; Aguila, B.; Perman, J.; Wang, S.; Huang, H.-Y.; Xiao, F.-S.; Ma, S. Pore Environment Control and Enhanced Performance of Enzymes Infiltrated in Covalent Organic Frameworks. J. Am. Chem. Soc. 2018, 140 (3), 984–992. https://doi.org/10.1021/jacs.7b10642.

(47) Deng, H.; Grunder, S.; Cordova, K. E.; Valente, C.; Furukawa, H.; Hmadeh, M.; Gándara, F.; Whalley, A. C.; Liu, Z.; Asahina, S.; Kazumori, H.; O'Keeffe, M.; Terasaki, O.; Stoddart, J. F.; Yaghi, O. M. Large-Pore Apertures in a Series of Metal-Organic Frameworks. Science 2012, 336 (6084), 1018–1023. https://doi.org/10.1126/science.1220131.

(48) Wang, S.; Chen, Y.; Wang, S.; Li, P.; Mirkin, C. A.; Farha, O. K. DNA-Functionalized Metal–Organic Framework Nanoparticles for Intracellular Delivery of Proteins. J. Am. Chem. Soc. 2019, 141 (6), 2215–2219. https://doi.org/10.1021/jacs.8b12705.

(49) Li, P.; Modica, J. A.; Howarth, A. J.; Vargas L, E.; Moghadam, P. Z.; Snurr, R. Q.; Mrksich, M.; Hupp, J. T.; Farha, O. K. Toward Design Rules for Enzyme Immobilization in Hierarchical Mesoporous Metal-Organic Frameworks. Chem 2016, 1 (1), 154–169. https://doi.org/10.1016/j.chempr.2016.05.001.

(50) Li, P.; Moon, S.-Y.; Guelta, M. A.; Lin, L.; Gómez-Gualdrón, D. A.; Snurr, R. Q.; Harvey, S. P.; Hupp, J. T.; Farha, O. K. Nanosizing a Metal–Organic Framework Enzyme Carrier for Accelerating Nerve Agent Hydrolysis. ACS Nano 2016, 10 (10), 9174–9182. https://doi.org/10.1021/acsnano.6b04996.

(51) Gascón, V.; Castro-Miguel, E.; Díaz-García, M.; Blanco, R. M.; Sanchez-Sanchez, M. In Situ and Post-Synthesis Immobilization of Enzymes on Nanocrystalline MOF Platforms to Yield Active Biocatalysts. J. Chem. Technol. Biotechnol. 2017, 92 (10), 2583–2593. https://doi.org/10.1002/jctb.5274.

(52) Carucci, C.; Bruen, L.; Gascón, V.; Paradisi, F.; Magner, E. Significant Enhancement of Structural Stability of the Hyperhalophilic ADH from Haloferax Volcanii via Entrapment on Metal Organic Framework Support. Langmuir 2018, 34 (28), 8274–8280. https://doi.org/10.1021/acs.langmuir.8b01037.

(53) Sun, Y.; Shi, J.; Zhang, S.; Wu, Y.; Mei, S.; Qian, W.; Jiang, Z. Hierarchically Porous and Water-Tolerant Metal–Organic Frameworks for Enzyme Encapsulation. Ind. Eng. Chem. Res. 2019, 58 (28), 12835–12844. https://doi.org/10.1021/acs.iecr.9b02164.

(54) Pan, Y.; Li, H.; Farmakes, J.; Xiao, F.; Chen, B.; Ma, S.; Yang, Z. How Do Enzymes Orient When Trapped on Metal–Organic Framework (MOF) Surfaces? J. Am. Chem. Soc. 2018, 140 (47), 16032–16036. https://doi.org/10.1021/jacs.8b09257.

(55) Chen, Y.; Han, S.; Li, X.; Zhang, Z.; Ma, S. Why Does Enzyme Not Leach from Metal–Organic Frameworks (MOFs)? Unveiling the Interactions between an Enzyme Molecule and a MOF. Inorg. Chem. 2014, 53 (19), 10006–10008. https://doi.org/10.1021/ic501062r.

(56) Yakushi, T.; Matsushita, K. Alcohol Dehydrogenase of Acetic Acid Bacteria: Structure, Mode of Action, and Applications in Biotechnology. Appl. Microbiol. Biotechnol. 2010, 86 (5), 1257–1265. https://doi.org/10.1007/s00253-010-2529-z.

(57) Kalscheuer, R.; Stölting, T.; Steinbüchel, A. 2006. Microdiesel: Escherichia Coli Engineered for Fuel Production. Microbiology 152 (9), 2529–2536. https://doi.org/10.1099/mic.0.29028-0.

(58) Qi, L.; Luo, Z.; Lu, X. Biomimetic Mineralization Inducing Lipase–Metal–Organic Framework Nanocomposite for Pickering Interfacial Biocatalytic System. ACS Sustain. Chem. Eng. 2019, 7 (7), 7127–7139. https://doi.org/10.1021/acssuschemeng.9b00113.

(59) Wang, H.; Han, L.; Zheng, D.; Yang, M.; Andaloussi, Y. H.; Cheng, P.; Zhang, Z.; Ma, S.; Zaworotko, M. J.; Feng, Y.; Chen, Y. Protein-Structure-Directed Metal–Organic Zeolite-like Networks as Biomacromolecule Carriers. Angew. Chem. 2020, 132 (15), 6322–6326. https://doi.org/10.1002/ange.202000299.

(60) Lian, X.; Chen, Y.-P.; Liu, T.-F.; Zhou, H.-C. Coupling Two Enzymes into a Tandem Nanoreactor Utilizing a Hierarchically Structured MOF. Chem. Sci. 2016, 7 (12), 6969–6973. https://doi.org/10.1039/C6SC01438K.

(61) Park, J.; Feng, D.; Zhou, H.-C. Dual Exchange in PCN-333: A Facile Strategy to Chemically Robust Mesoporous Chromium Metal–Organic Framework with Functional Groups. J. Am. Chem. Soc. 2015, 137 (36), 11801–11809. https://doi.org/10.1021/jacs.5b07373.

(62) Chen, W.; Yang, W.; Lu, Y.; Zhu, W.; Chen, X. Encapsulation of Enzyme into Mesoporous Cages of Metal–Organic Frameworks for the Development of Highly Stable Electrochemical Biosensors. Anal. Methods 2017, 9 (21), 3213–3220. https://doi.org/10.1039/C7AY00710H.

(63) Tani, A.; Sakai, Y.; Ishige, T.; Kato, N. Thermostable NADP+-Dependent Medium-Chain Alcohol Dehydrogenase from Acinetobacter Sp. Strain M-1: Purification and Characterization and Gene Expression InEscherichia Coli. Appl. Environ. Microbiol. 2000, 66 (12), 5231–5235. https://doi.org/10.1128/AEM.66.12.5231-5235.2000.

(64) Zhao, Q.; Hou, Y.; Gong, G.-H.; Yu, M.-A.; Jiang, L.; Liao, F. Characterization of Alcohol Dehydrogenase from Permeabilized Brewer's Yeast Cells Immobilized on the Derived Attapulgite Nanofibers. Appl. Biochem. Biotechnol. 2010, 160 (8), 2287–2299. https://doi.org/10.1007/s12010-009-8692-y.

3.0 Chapter 2: A study on the effectiveness of PCN-333(Fe) as a drug delivery device for IFN-γ and its effect on Human Kupfer Cell Viability

3.0.1 Abstract

Metal-organic frameworks or MOFs have shown great potential for use as a drug carrier given the natural characteristics of their porosity and ability to be functionalized. These attributes

allow for easy loading, sustained release, and the capability to be site directed either specifically by the conjugation of targeting molecules or non-specifically given that MOFs can be chosen that disintegrate or travel to specific locations in the body naturally. This non-specific function can be leveraged to deliver drug molecules throughout the body or directly to localized cells depending on the method of administration. Despite the many benefits of MOFs, their use in practice has not yet been widely accepted. This can be attributed to lack of understanding surrounding the complex and its effects on the surrounding cellular environment. In this work we seek to expand our field's understanding of the use of MOFs as delivery devices by immobilizing the protein interferon-γ (IFN-γ) on the MOF PCN-333(Fe) to observe the effect of its presence and the delivery of the immobilized protein to human mesenchymal stem cells. In doing so, we report that the MOF shows continued biocompatibility consistent with literature while providing an excellent scaffolding for immobilization and release of IFN-γ to surrounding cells.

3.0.2 Introduction

Recent years have seen a significant increase in the study of metal-organic frameworks (MOFs) since their foundational introduction by Omar Yagi and coworkers.[23,27,57,61,102–104] These porous crystalline particles are often produced on the nanoscale and due to their interchangeable parts, are vastly customizable.[23] This ability to selectively choose components and synthesize tailor-made MOFs allows these particles to be functionalized as well as have their three-dimensional size and shape manipulated.[21,104] The functionalization can be multi-faceted allowing for what is called a "tandem reaction" where more than one reaction takes place in the same space.[97,105] Coupling that with their incredible stability in an array of solvents,

temperatures, and pH conditions, makes MOFs powerful tools for catalysis.[22,63] This is further promoted by the open pores and large surface areas of MOFs which allow materials to move into the particles providing a high loading capacity and surface area.[21] This effect is excellent for reactions, allowing the free flow of reactants and products to reaction sites. This trait has also been exploited to encapsulate or trap objects, which can be as big as proteins or as small as gas particles making MOFs prominent devices for gas storage, drug delivery, and protein immobilization and/or encapsulation.[23]

Protein immobilization and encapsulation is made possible by the fluid nature of proteins with their ability to fold and unfold as well as the inherent interactions arising between the chemical groups on MOF particles and the proteins. Immobilization is a relatively simple process where the charged portions of proteins interact with the positively charged bare node sites on the framework and become coordinated to that site.[32,106] Encapsulation is a more complicated process where the protein either moves into the framework via diffusion or is placed in solution with MOF reactants and the framework is built up around it. The former is called post-synthetic encapsulation (PSE) and the latter is known as De-novo encapsulation or DNE.[35] In both PSE and DNE, proteins are held in place physically by the surrounding framework, but they are also held in place by intermolecular forces such as London dispersion forces (LDFs), dipole-dipole interactions, and hydrogen bonding between the framework and the protein14,16.[32,37]

Protein immobilization and encapsulation using MOFs has been shown to allow improved reaction kinetics while protecting the housed protein from extreme conditions that would otherwise cause the protein to denature and become inactive.[28,56,97] This includes reactions taking place at temperatures above 60 degrees Celsius, in organic solvents, and at both high

and low pH.[52] We demonstrate this effect in a recent publication encapsulating and monitoring the loading and reaction kinetics of Alcohol Dehydrogenase in the MOF PCN-333(Fe).[35] While catalytic reactions are a major interest in MOF-protein immobilization, another key use of MOF-protein immobilization is in drug and protein delivery. This is made clear in a recent work by luzuriaga et. al. where it's shown that proteinaceous vaccines can be both protected/insulated from the outside environment as well as carried by site-directed delivery to a given location even inside the cell.[33]

The delivery of proteins is a very promising area of study with the ability to have a dramatic impact on those suffering from genetic dispositions. Human mesenchymal stromal cells (hMSCs) are an excellent model cell and are particularly interesting to cellular therapy programs due to their function as an immunosuppressant.[107] During tissue damage, hMSCs have the ability to secrete paracrine and anti-inflammatory factors to repair tissue.[108–110] In addition, hMSCs contribute not only to the repair of damaged tissues but also possess remarkable immunomodulatory activity by producing anti-inflammatory and immunosuppressive factors.[111–116] This has led to hMSCs to becoming a promising tool for new medical applications and therapies in the treatment of diverse diseases and disorders, such as graft-versus-host disease, inflammatory diseases, and autoimmune disorders.[117,118]

It has been shown that the immunosuppressive properties of hMSCs rely on the existence of IFN-γ in the microenvironment.[114] This signaling protein is a potent pro-inflammatory cytokine produced by CD4+ lymphocytes, natural killer cells (NKT) cells, and macrophages. Because of this function, IFN-γ plays an essential and complex role in innate and adaptive immune responses in viral infections, bacteria, protozoa, and graft-versus-host disease (GVHD).[115,116] A

recent study by Croitoru-Lamoury et. al. showed that IFN-γ has the ability to modulate the immune properties and differentiation potential of hMSCs.[117] However, in spite of the fact that the existence of IFN-γ increase the immunosuppressive properties of hMSCs, the transient effects of IFN-γ may limit the potential of hMSCs to modulate immune responses for more than a few days in cell environments that do not expose the cells to the required concentrations of IFN-γ, such as in chronic inflammatory states.[119] Therefore, providing a means of locally concentrating and sustaining the presentation of IFN-γ to hMSCs may significantly enhance the immunomodulatory potential of the cells. In this paper we seek to show that the immobilization and delivery of factors, specifically IFN-γ with PCN-333 is both an effective means for delivery to potentiate hMSC immunomodulatory activity.

3.1.0 Experimental Section

3.1.1 Synthesis of PCN-333(Fe)

Synthesis of PCN-333(Fe) The precursor 4,4′,4′′-s-triazine-2,4,6-triyl-tribenzoic acid (H3TATB) and MOF PCN-333(Fe) were synthesized according to the method described in the work by Park et. al. 2015.[98] In a 15 mL reaction vessel, we combined 60 mg H3TATB, 60 mg anhydrous FeCl3 (III), 0.6 mL TFA, and 10 mL DMF. The vessel was then sealed and placed in an oven at 150 °C for 12 hours. Brown precipitate formed and was collected by centrifugation. Product was washed several times each by DMF, acetone, and water with centrifugation after each step to collect. Water was then exchanged with acetone three times before activation in an oven at 70°C overnight. The product was then confirmed via X-ray diffraction (Figure 6a). Size and shape where also determined via SEM and the use of a Horiba LA-950 particle size analyzer. These results can be seen in figures 1b and 1c respectively.

3.1.2 Immobilization of IFN-γ with PCN-333(Fe)

A loading solution of PCN-333 and IFN -γ was combined with a final concentration 0.1 mg/mL IFN-γ and either 0.5 or 1 mg/mL PCN-333 depending on the test. This solution was vortexed and allowed to sit at 4°C for 24 hours. The solution was then removed after gentle centrifugation leaving the immobilized IFN-γ and PCN-333. Loading was determined by UV absorption at 280nm by HPLC.

3.1.3 hMSC Viability

For the hMSCs viability, PrestoBlueTM cell viability assay from Invitrogen (Cat. #A13261) was used. hMSCs (10000 cells/cm2) were seeded on a 96 well-plate, and cell viability was measured after 3 and 6 days of culture as described in our previous works.[120–122] Briefly, the cell culture medium was removed, and 100 µL per well containing 90% fresh cell medium and 10% PrestoBlue reagent were added. The plate was incubated for 3 hours, and the fluorescence intensity measurement was determined using a BioTek Multi-Mode Microplate Reader (Model SynergyTM 2) with excitation/emission of 560/590 nm. Data were summarized per culture conditions.

Fluorescent staining was performed to detect the blue fluorescent dye Hoechst 33 342 which was purchased from Invitrogen (Ref. #H3570). This dye stains nucleic acid making it permeable to the cell. The red-orange fluorescent dye ActinRedt 555 Ready Probest was purchased from Invitrogen (Ref. #37112) was also monitored, which is selective to Actin F (a fundamental component of the cellular cytoskeleton). After three days of culture, the cell medium was removed, and the cells were fixed with 4% formaldehyde solution for 15 minutes. The samples were washed several times with PBS followed by adding Triton X100 for 10 minutes and they

were then washed 3 times. ActinRedt 555 was first added and incubated for 30 minutes. Then, Hoechst 33 342 was added for 10 minutes and protected from light by aluminum foil. Both dyes were washed 5 times with PBS before and after being added. For cell imaging, Leica inverted fluorescence microscope was used with a standard DAPI filter (excitation/emission of 350/461 nm) for Hoechst 33 342, and a standard TRITC filter (excitation/emission of 540/565 nm) for ActinRedt 55.

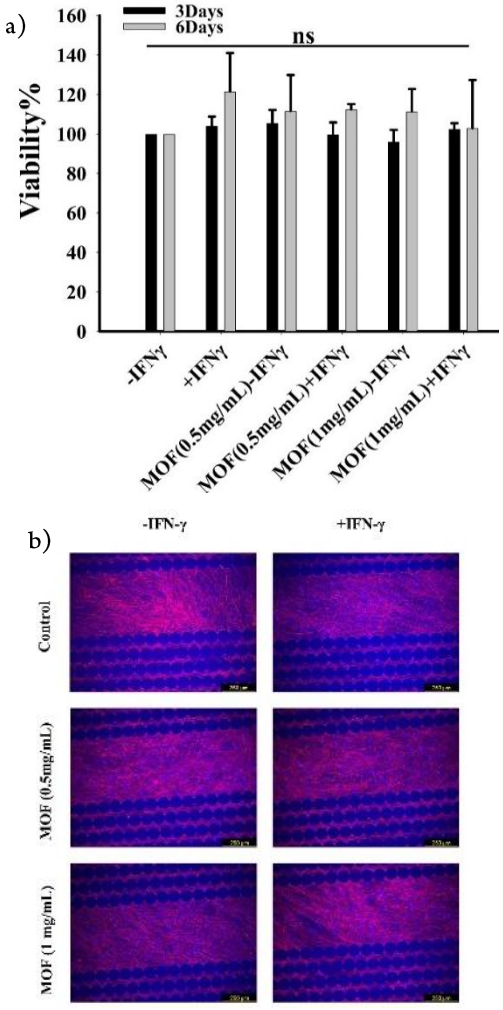

Figure 8 a) PrestoBlue Viability assay for cultured hMSCs after 3 and 6days cells cultured. b) Fluorescence microscopy images of hMSCs nuclei and actin cytoskeleton, labeled with Hoechst and Actin Red.

3.1.4 Real-time monitoring of hMSCs behavior

An xCELLigence Real-Time Cell Analyzer (RTCA S16) instrument from ACEA Biosciences Inc. (Cat. #00380601430) was used to measure real-time cell behavior. hMSCs at a concentration of 5000 cells/cm2 were seeded on the wells of an ACEATM E-Plate L16 (Cat. #00300600890, cell growth area of 0.32 cm2 per well), on each condition (hMSCs cultured with and without IFN-γ supplemented in the culture medium, MOF(0.5mg/mL), MOF(0.5mg/mL) + IFN-γ, MOF(1mg/mL), and MOF(1mg/mL) + IFN-γ. The xCELLigence instrument was configured as described in our previous works35,36. Briefly, the xCELLigence RTCA S16 was placed inside the incubator to allow the device to warm up for at least 2 hours before use. The RTCA S16 was set up to perform readings every 10 minutes for a period of 72 hours of cell culture.

3.1.5 Immunomodulatory factor expression of hMSC's

For the hMSCs immunomodulatory factor expression, hMSCs (5000 cells/cm2) were seeded on each well of a 24 well-plate, and the IDO activity was measured after 3 and 6 days of culture (changing the cells medium every 2 days) as described in our previous works.[120,122,123] Briefly, cell supernatant 100 µL was mixed with 100 µL standard assay mixture consisting of (potassium phosphate buffer (50mM, pH 6.5), ascorbic acid (40 mM, neutralized with NaOH), catalase (200 µg/ml), methylene blue (20 µ M), L-tryptophan (400 µM)). The mixture was kept at 37°C in a humidified incubator with 5% CO2 for 30 min (in a dark environment to protect solutions from light) to allow IDO to convert L-tryptophan to N-formyl-kynurenine. After that, the reaction was stopped by adding 100 µL trichloroacetic acid 30% (wt/vol) and incubating for 30 min at 58 °C. After hydrolysis of N-formyl-kynurenine to kynurenine, 100µL of mixed cell supernatant/standard transfer into a well of a 96-well microplate, followed by adding 100 µL

per well of 2% (w/v) p-dimethylaminobenzaldehyde in acetic acid. Absorbance was read at 490 nm at the endpoint using a BioTek Synergy 2 spectrophotometer (Synergy LX Multi-Mode Reader from BioTek® Model SLXFA).

3.1.6 hMSC Differentiation

hMSCs differentiation was induced by their culture with differentiation media (Osteogenic and Adipogenic media). Control cultures were grown in a regular cell expansion medium. Briefly, hMSCs (10,000 cells/cm2) were seeded on each condition prepared on 24 well-plates and grown for 6 days in expansion medium (MEM Alpha (1X) supplemented with L-glutamine, ribonucleosides, and deoxyribonucleosides) containing 20% fetal bovine serum, 1.2% penicillin-streptomycin, and 1.2% L-glutamine at 37 °C in a humidified incubator with 5% CO2. After the cells reached at least 50% confluency, they were exposed to a differentiation medium. For osteogenic differentiation, hMSCs were cultured in the differentiation medium composed of DMEM low glucose, 10% fetal bovine serum,1% penicillin, 1% L-Glutamin, 50 µM ascorbic acid (50mg/10ml) (Sigma, Cas Number: 50-81-7), 10 mM β-glycerophosphate (e.g., Sigma, CAS Number: 154804-51-0, G9422), and 100nM dexamethasone (e.g., Sigma, CAS Number 50-02-2). The medium was replaced every 2-3 days. After 8 days of culture, cells were fixed with 10% formaldehyde. For osteogenic differentiation, Alizarin Red S (Sigma, CAS Number 130-22-3) staining solution was prepared by adding 2g Alizarin Red S in 100 mL water mixed. The pH was adjusted to 4.1– 4.3 by the addition of Ammonium Hydroxide, as necessary. Alizarin Red S solution was added to the fixed cells, then incubated at room temperature in the dark (covered with aluminum foil) for 15 minutes. The staining solution was removed and rinsed 3 times with PBS. The samples were analyzed immediately under the microscope to detect calcium deposits.

For adipogenic differentiation, hMSCs were cultured in the differentiation medium consisting of DMEM high glucose supplemented with 10% fetal bovine serum, 1% penicillin, 1% L-glutamin, 1 µM dexamethasone (e.g., Sigma, CAS Number 50-02-2), 0.01 mg/mL insulin (Sigma-Aldrich, Catalog No. I2643), 0.5 mM 3-isobutyl-1-methylxanthine (IBMX) (e.g., Sigma, CAS Number: 28822-58-4, I5879), and 100µM indomethacin (Sigma, CAS Number: 53-86-1). The medium was replaced every 2-3 days. After 8 days of culture, cells were fixed with 10% formaldehyde, stained with 0.5% (w/v) Oil Red O (Sigma-Aldrich, Catalog Number: O0625) in 100% isopropanol, incubated at room temperature for 30 minutes, and protected from light. The cell monolayer was washed 2 times with PBS. The sample was analyzed under a light microscope to detect lipid vesicles that appeared in bright red. A one-way analysis of variance (ANOVA) was performed drawing comparisons among multiple groups. A p-value < 0.05 was considered statistically significant. The statistical analysis was done using SigmaPlot software version 14.

3.2.0 Results and Discussion

3.2.1 Characterization of PCN-333(Fe)

The successful synthesis of PCN-333(Fe) was confirmed via powder X-ray Diffraction, showing a pattern consistent with previous works (Figure 1a).[35,98] The product was then observed under SEM (figure 1b), which shows that the product is roughly spherical in nature. Upon size analysis using the Horiba LA-950, it was determined that the average particle size was 17.8 µm while the mode was18.6 µm. The standard deviation was determined to be 2.7.

3.2.2 Immobilization of IFN-X with PCN-333(Fe)

To immobilize IFN- γ, a solution of 0.1 mg/ml IFN- γ and either 0.5 or 1 mg/ml PCN-333 in 20mM pH 7 HEPES buffer was prepared. The solution was lightly vortexed and allowed to sit at

4°C for 24 hours. The solution was then lightly vortexed and subsequently centrifuged at 1000 rpm for 1 minute. The supernatant was removed, and the sample was ready for incorporation

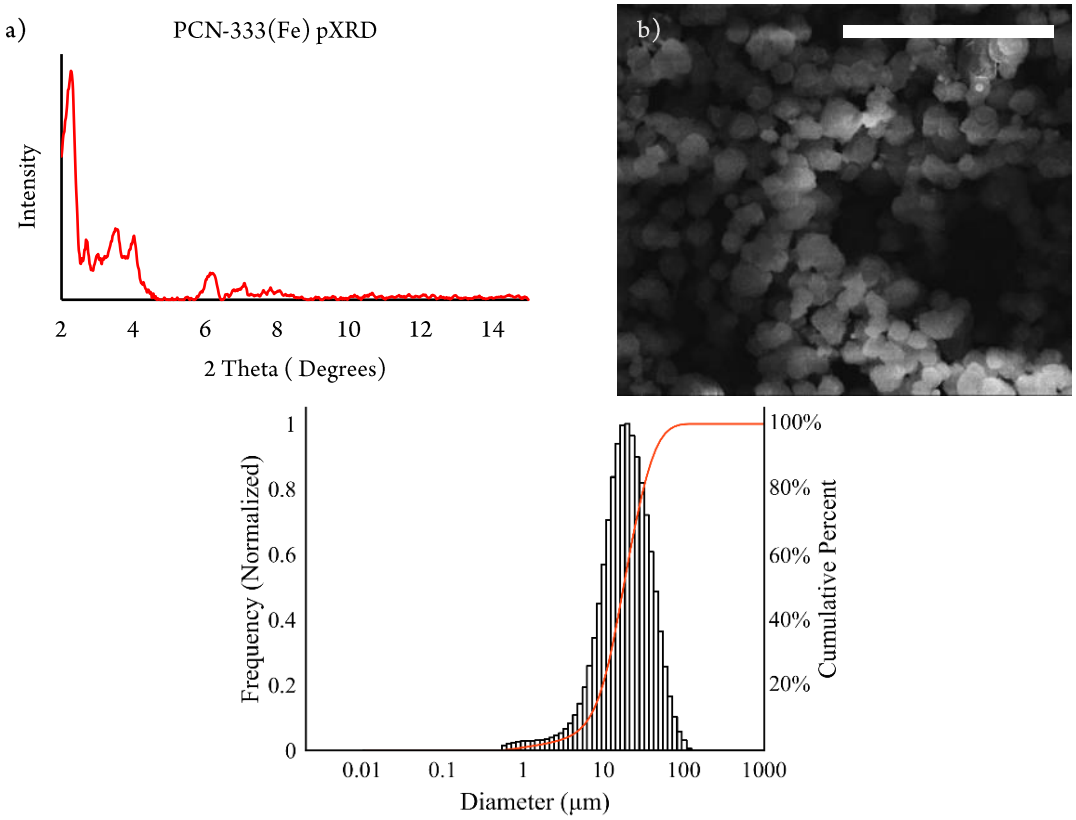

Figure 9 *a) pXRD of synthesized PCN-333 (Fe) b) SEM image of synthesized PCN-333(Fe) with scale bar representing 40 µm. c) Size distribution of synthesized PCN-333(Fe)(black) and cumulative percentage of product (red).*

into the cell media. Percent immobilization was then determined by absorbance of the supernatant at 280 nm against controls via HPLC. This showed the percent immobilization to be 39% in the 1mg/ml sample of PCN-333(Fe) and 34% for the 0.5mg/mL PCN-333(Fe) sample.

3.2.3 PrestoBlue Viability Assay

Cytotoxicity was evaluated by monitoring the activity of the reagent Presto Blue. Using this reagent, cell viability was measured after 3 and 6 days of culturing hMSCs cells under each condition. Those conditions being with and without IFN-γ supplemented in the culture medium,

MOF (0.5mg/mL), MOF (0.5mg/mL) + IFN-γ, MOF (1mg/mL), and MOF (1mg/mL) + IFN-γ. The positive control group selected contained cell medium lacking IFN-γ. The fluorescence intensity of the positive control was normalized to 100%. All other conditions were assessed in relation to the positive control. Figure 2a shows IFN-γ supplemented in cell medium have higher cell viability of about 2% and 20% than the control in 3 and 6 days, respectively. This result shows that IFN-γ supplemented does not affect cell viability. As shown in Figure 2a, MOF (0.5 mg/mL) has a 20% higher cell viability than MOF in higher concentrations (1mg/mL) after 3 days. However, MOF (0.5 mg/mL and 1 mg/mL) shows the same cell viability after 6 days. Therefore, MOF in both concentrations (0.5 and 1 mg/mL) does not surpass the cell viability compared to control. Regarding the MOF (0.5 mg/mL) + IFN-γ, the cell viability increased 10% after 6 days compared to 3 days. However, the cell viability of MOF (1 mg/mL) + IFN-γ did not change after 6 days. These results show that MOF alone and MOF with IFN-γ do not have any cytotoxic effect on hMSCs, while MOF (0.5mg/mL) showed better biocompatibility than the MOF (1mg/mL). Fluorescence microscopy images of hMSCs nuclei labeled with Hoechst of cells attached to the different surfaces after 72 hours validate the findings of cell viability of hMSCs in each condition.

3.2.4 Real-time monitoring of cell behavior and proliferation

In this study, hMSCs at 25000 cells/cm2 were cultured on E-Plate 16 to evaluate the real-time behavior of the cells during the first 72 hours of culture. The effect of the presence and absence of the IFN-γ in the cell medium, MOF (0.5mg/mL), MOF (0.5mg/mL) + IFN-γ, MOF (1mg/mL), and MOF (1mg/mL) + IFN-γ was also evaluated. As a control surface, we evaluated growth without IFN-γ. An xCELLigence RTCA S16 biosensor system was used to measure cell

proliferation and growth. This system constantly measures the impedance difference caused by cells attache d to microsensors present in culture plates (E-plates 16) and is monitored by microchips attached under the wells. In this way, the impedance difference is translated into a parameter known as the Cell Index (CI). Therefore, the higher the CI, the greater the number of cells adhered to the bottom of the well36 . Based on our previous study, the results indicate two cell behavior phases: a cell adhesion and a cell proliferation phase, after 30 hours and between 30-72 hours of culture, respectively38.

The Figure 3 shows the CI values as a function of the first 72 hours of culture for the 6 experimental conditions. The Figure shows a slow cell adhesion stage in the evaluated period, reaching a maximum peak of around 9 hours. CI values reached a maximum of 8 CI units. Compared to the samples without the IFN-γ, cell adhesion has a lower CI value, including MOF (0.5 and 1mg/mL) in the cells medium. In addition, cells including MOF (0.5mg/mL) + IFN-γ have

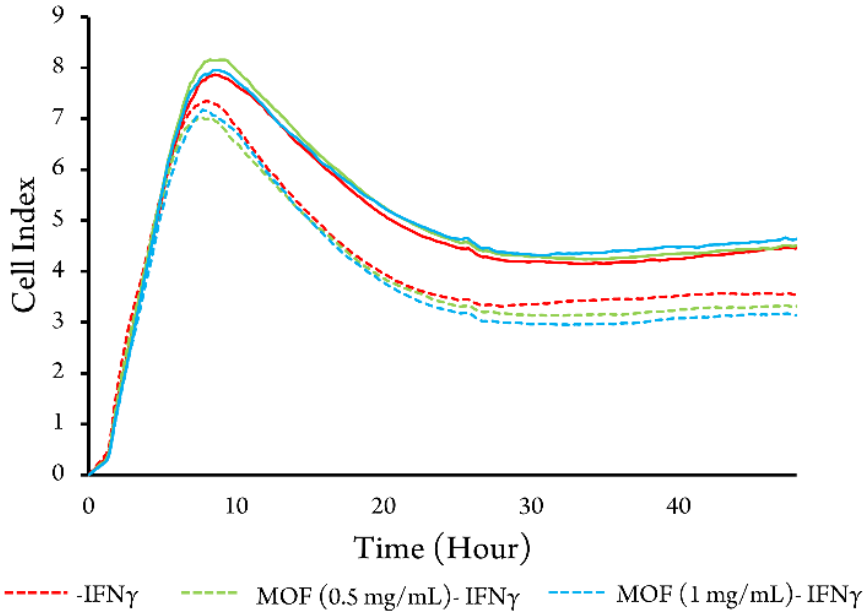

Figure 10 Real-time monitoring of hMSCs after 72 hours.

a higher CI value compared to other conditions. This finding indicates that MOF (0.5 and 1 mg/mL) with IFN-γ does not negatively effect on cell adhesion.

3.2.5 IDO Assay

Indoleamine 2,3-dioxygenase (IDO) is a cytosolic heme protein important for immuno-regulatory functions.[124,125] It's presence can be evaluated by measuring the concentration of kynurenine, which is a known catalyzer that helps convert L-tryptophan to kynurenine.[124,126] The ability of IFN-γ to induce IDO expression in hMSCs was compared with and without IFN-γ supplemented in the culture medium, MOF (0.5mg/mL), MOF (0.5mg/mL) + IFN-γ, MOF (1mg/mL), and MOF (1mg/mL) + IFN-γ supplemented in the cell culture medium after 3 days and 6 days. Results for IDO activity is summarized in Figure 4. These results show that IFN-γ supplemented in cell medium increases the IDO activity 4 times higher than the cell medium

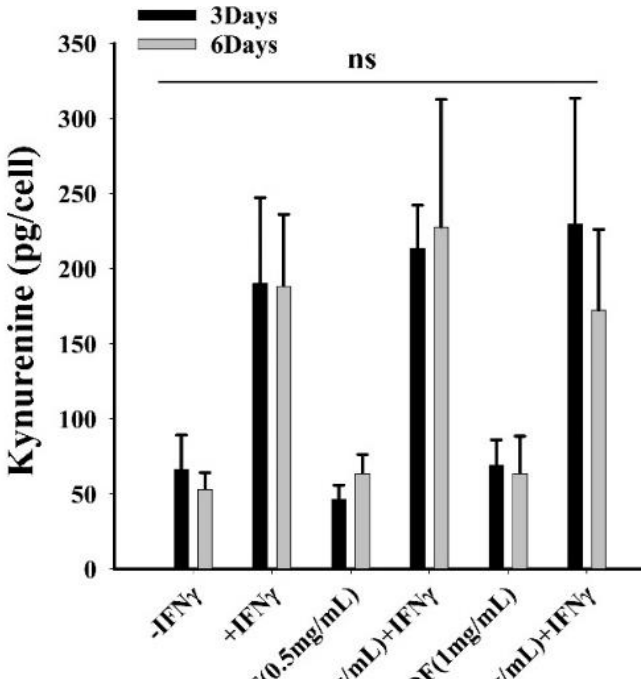

Figure 11 *Cells immunomodulatory potential by IDO activity for hMSCs as a measure of picograms of kynurenine produced by cells cultured after 3 and 6 days.*

without IFN-γ. These results are in line with the study done by Kwee et al., indicating the IDO activity correlated with the amount of IFN-γ.[127]

With regard to MOF (0.5mg/mL) and MOF (1mg/mL) in cells medium, the results show no differences compared to with IFN-γ. This result indicates that MOF alone does not affect IDO activity. In addition, the MOF (0.5mg/mL) + IFN-γ show a higher IDO activity after 6 days compared to 3 days, which may show the presence of more IFN-γ in the cell medium after 6 days. However, MOF (1 mg/mL) + IFN-γ show less IDO activity after 6 days compared with 3 days, which can be related to the amount of IFN-γ encapsulated in MOF and can be expected when there are more potential binders in solution, given that there are two times the amount of MOF particles. These results indicate that MOF (0.5mg/mL) + IFN-γ may have the ability to release IFN-γ through passage of time. While this may also be the case for MOF (1mg/mL) + IFN-γ, a longer time-course study would be required.

3.2.6 Cells differentiation assay

The ability of hMSCs to differentiate into osteogenic and adipogenic lineages cells was induced by replacing the growth medium with the differentiation medium. The differentiation ability of hMSCs was evaluated to confirm the multipotentiality of hMSCs. After 10 days of incubation, cell functions associated with osteoblast differentiation (calcium deposition) and adipogenic differentiation were evaluated. Mineralization was also characterized from microscope images. Figure 5 shows that there are areas visible with red and purple, indicating the formation of the calcified regions and adipocyte-like cells, respectively. Figure 5 also shows that control cells show a calcium deposit formed by the clustering of cells due to the strong staining with Alizarin red even with and without IFN-γ, which indicates osteogenic differentiation of cells. The same

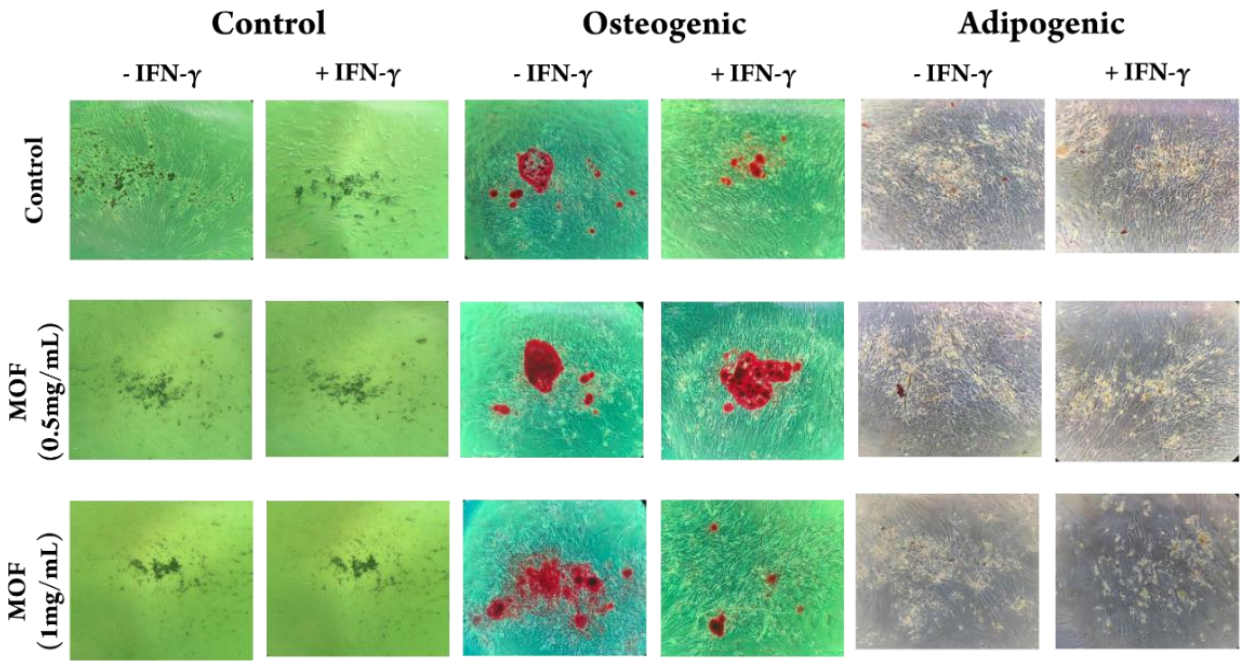

Figure 12 hMSCs differentiation. control cells inducing by normal expansion medium. Osteogenic differentiations were stained by Alizarin Red. Adipogenic differentiation were stained by Oil Red.

results were found for MOF (0.5 and 1mg/mL) and MOF (0.5 and 1mg/mL) + IFN-γ, as shown in Figure 5. Also, Figure 5 shows that control cells, even with and without IFN-γ, have the ability to differentiate into adipogenic cells, which is where the cells changed from long spindle-shaped to flattened round or polygonal cells. In addition, Figure 5 shows that the treatment with IFN-γ encapsulated in MOFs had no inhibitory effect on the osteogenic and adipogenic differentiation of hMSCs. As shown in Figure 5, no staining was observed on cells cultured in regular expansion medium.

3.3.0 Conclusions from experiment

In this work, we tested the viability of the use of the metal-organic framework PCN-333(Fe) as a carrier device for the delivery of IFN-γ to human mesenchymal stem cells and monitored the immunomodulatory activity of these cells to determine its efficacy. From our results, we show that, likewise to other publications, the PCN-333(Fe) has little to no effect on cell viability and

the particle is not cytotoxic. While the increased concentration of the particles did lead to a slightly lower cell count early in the experiment, the percent viability after 6 days was comparable to that of the lower concentration. Additionally, when introduced to the cell differentiation assay, the experimental group containing the MOF particles showed no variance and continued to differentiate appropriately. When measuring the efficiency of IFN-γ and IDO in the presence of MOF, the controls containing the particle had no effect on either test showing it to be an ideal carrier, not interfering with the biological pathways. Finally, the successful release of IFN-γ compared to the control group over the course of 3 and 6 days shows that the MOF particle is an excellent device for the delivery of small proteins. While there was a smaller distribution of IFN-γ to cells in the 1.0mg/mL sample, this can be attributed to the increased number of competing factors to bind to the proteins in solution which in turn cause the observed decrease in IFN-γ activity. The results from this work show that PCN-333(Fe) are suitable delivery devices for small protein to cells in vitro with little to no side effects on the surrounding environment or the cellular ability to reproduce or differentiate and have the added benefit of providing a sustained release of loaded materials to nearby cells. Future studies will be needed to further understand the viability of this delivery method, but the results from this work suggest that the use of MOFs as a delivery device is a reasonable alternative to conventional methods of chemical introduction.

3.4.0 References

(65) Eddaoudi, M.; Li, H.; Yaghi, O. M. Highly Porous and Stable Metal−Organic Frameworks: Structure Design and Sorption Properties. J. Am. Chem. Soc. 2000, 122 (7), 1391–1397. https://doi.org/10.1021/ja9933386.

(66) Kim, J.; Chen, B.; Reineke, T. M.; Li, H.; Eddaoudi, M.; Moler, D. B.; O'Keeffe, M.; Yaghi, O. M. Assembly of Metal−Organic Frameworks from Large Organic and Inorganic Secondary

Building Units: New Examples and Simplifying Principles for Complex Structures. J. Am. Chem. Soc. 2001, 123 (34), 8239–8247. https://doi.org/10.1021/ja010825o.

(67) Eddaoudi, M.; Moler, D. B.; Li, H.; Chen, B.; Reineke, T. M.; O'Keeffe, M.; Yaghi, O. M. Modular Chemistry: Secondary Building Units as a Basis for the Design of Highly Porous and Robust Metal−Organic Carboxylate Frameworks. Acc. Chem. Res. 2001, 34 (4), 319–330. https://doi.org/10.1021/ar000034b.

(68) Eddaoudi, M.; Kim, J.; Rosi, N.; Vodak, D.; Wachter, J.; O'Keeffe, M.; Yaghi, O. M. Systematic Design of Pore Size and Functionality in Isoreticular MOFs and Their Application in Methane Storage. Science 2002, 295 (5554), 469–472. https://doi.org/10.1126/science.1067208.

(69) Wang, Q.; Astruc, D. State of the Art and Prospects in Metal–Organic Framework (MOF)-Based and MOF-Derived Nanocatalysis. Chem. Rev. 2020, 120 (2), 1438–1511. https://doi.org/10.1021/acs.chemrev.9b00223.

(70) Li, P.; Chen, Q.; Wang, T. C.; Vermeulen, N. A.; Mehdi, B. L.; Dohnalkova, A.; Browning, N. D.; Shen, D.; Anderson, R.; Gómez-Gualdrón, D. A.; Cetin, F. M.; Jagiello, J.; Asiri, A. M.; Stoddart, J. F.; Farha, O. K. Hierarchically Engineered Mesoporous Metal-Organic Frameworks toward Cell-Free Immobilized Enzyme Systems. Chem 2018, 4 (5), 1022–1034. https://doi.org/10.1016/j.chempr.2018.03.001.

(71) Phipps, J.; Chen, H.; Donovan, C.; Dominguez, D.; Morgan, S.; Weidman, B.; Fan, C.; Beyzavi, H. Catalytic Activity, Stability, and Loading Trends of Alcohol Dehydrogenase Enzyme Encapsulated in a Metal–Organic Framework. ACS Appl. Mater. Interfaces 2020, 12 (23), 26084–26094. https://doi.org/10.1021/acsami.0c06964.

(72) L. Ramos, T.; Sánchez-Abarca, L. I.; Muntión, S.; Preciado, S.; Puig, N.; López-Ruano, G.; Hernández-Hernández, Á.; Redondo, A.; Ortega, R.; Rodríguez, C.; Sánchez-Guijo, F.; del Cañizo, C. MSC Surface Markers (CD44, CD73, and CD90) Can Identify Human MSC-Derived Extracellular Vesicles by Conventional Flow Cytometry. Cell Commun. Signal. 2016, 14 (1), 2. https://doi.org/10.1186/s12964-015-0124-8.

(73) Brooke, G.; Cook, M.; Blair, C.; Han, R.; Heazlewood, C.; Jones, B.; Kambouris, M.; Kollar, K.; McTaggart, S.; Pelekanos, R.; Rice, A.; Rossetti, T.; Atkinson, K. Therapeutic Applications of Mesenchymal Stromal Cells. Semin. Cell Dev. Biol. 2007, 18 (6), 846–858. https://doi.org/10.1016/j.semcdb.2007.09.012.

(74) Pittenger, M. F.; Discher, D. E.; Péault, B. M.; Phinney, D. G.; Hare, J. M.; Caplan, A. I. Mesenchymal Stem Cell Perspective: Cell Biology to Clinical Progress. Npj Regen. Med. 2019, 4 (1), 1–15. https://doi.org/10.1038/s41536-019-0083-6.

(75) Watt, F. M.; Huck, W. T. S. Role of the Extracellular Matrix in Regulating Stem Cell Fate. Nat. Rev. Mol. Cell Biol. 2013, 14 (8), 467–473. https://doi.org/10.1038/nrm3620.

(76) Hynes, R. O. The Extracellular Matrix: Not Just Pretty Fibrils. Science 2009, 326 (5957), 1216–1219. https://doi.org/10.1126/science.1176009.

(77) Lortat-Jacob, H. The Molecular Basis and Functional Implications of Chemokine Interactions with Heparan Sulphate. Curr. Opin. Struct. Biol. 2009, 19 (5), 543–548. https://doi.org/10.1016/j.sbi.2009.09.003.

(78) Brizzi, M. F.; Tarone, G.; Defilippi, P. Extracellular Matrix, Integrins, and Growth Factors as Tailors of the Stem Cell Niche. Curr. Opin. Cell Biol. 2012, 24 (5), 645–651. https://doi.org/10.1016/j.ceb.2012.07.001.

(79) Klinker, M. W.; Marklein, R. A.; Lo Surdo, J. L.; Wei, C.-H.; Bauer, S. R. Morphological Features of IFN-γ-Stimulated Mesenchymal Stromal Cells Predict Overall Immunosuppressive Capacity. Proc. Natl. Acad. Sci. U. S. A. 2017, 114 (13), E2598–E2607. https://doi.org/10.1073/pnas.1617933114.

(80) Ijzermans, J. N.; Marquet, R. L. Interferon-Gamma: A Review. Immunobiology 1989, 179 (4–5), 456–473. https://doi.org/10.1016/S0171-2985(89)80049-X.

(81) Liu, Y.; Wang, L.; Kikuiri, T.; Akiyama, K.; Chen, C.; Xu, X.; Yang, R.; Chen, W.; Wang, S.; Shi, S. Mesenchymal Stem Cell–Based Tissue Regeneration Is Governed by Recipient T Lymphocytes via IFN-γ and TNF-α. Nat. Med. 2011, 17 (12), 1594–1601. https://doi.org/10.1038/nm.2542.

(82) Croitoru-Lamoury, J.; Lamoury, F. M. J.; Caristo, M.; Suzuki, K.; Walker, D.; Takikawa, O.; Taylor, R.; Brew, B. J. Interferon-γ Regulates the Proliferation and Differentiation of Mesenchymal Stem Cells via Activation of Indoleamine 2,3 Dioxygenase (IDO). PloS One 2011, 6 (2), e14698. https://doi.org/10.1371/journal.pone.0014698.

(83) Castilla-Casadiego, D. A.; García, J. R.; García, A. J.; Almodovar, J. Heparin/Collagen Coatings Improve Human Mesenchymal Stromal Cell Response to Interferon Gamma. ACS Biomater. Sci. Eng. 2019, 5 (6), 2793–2803. https://doi.org/10.1021/acsbiomaterials.9b00008.

(84) Zimmermann, J. A.; Hettiaratchi, M. H.; McDevitt, T. C. Enhanced Immunosuppression of T Cells by Sustained Presentation of Bioactive Interferon-γ Within Three-Dimensional Mesenchymal Stem Cell Constructs. Stem Cells Transl. Med. 2017, 6 (1), 223–237. https://doi.org/10.5966/sctm.2016-0044.

(85) Castilla-Casadiego, D. A.; Reyes-Ramos, A. M.; Domenech, M.; Almodovar, J. Effects of Physical, Chemical, and Biological Stimulus on h-MSC Expansion and Their Functional Characteristics. Ann. Biomed. Eng. 2020, 48 (2), 519–535. https://doi.org/10.1007/s10439-019-02400-3.

(86) Pinzon-Herrera, L.; Mendez-Vega, J.; Mulero-Russe, A.; Castilla-Casadiego, D. A.; Almodovar, J. Real-Time Monitoring of Human Schwann Cells on Heparin-Collagen Coatings

Reveals Enhanced Adhesion and Growth Factor Response. J. Mater. Chem. B 2020, 8 (38), 8809–8819. https://doi.org/10.1039/D0TB01454K.

(87) Cifuentes, S. J.; Priyadarshani, P.; Castilla-Casadiego, D. A.; Mortensen, L. J.; Almodóvar, J.; Domenech, M. Heparin/Collagen Surface Coatings Modulate the Growth, Secretome, and Morphology of Human Mesenchymal Stromal Cell Response to Interferon-Gamma. J. Biomed. Mater. Res. A 2021, 109 (6), 951–965. https://doi.org/10.1002/jbm.a.37085.

(88) Castilla-Casadiego, D. A.; Timsina, H.; Haseli, M.; Pinzon-Herrera, L.; Chiao, Y.-H.; Wickramasinghe, S. R.; Almodovar, J. Methods for the Assembly and Characterization of Polyelectrolyte Multilayers as Microenvironments to Modulate Human Mesenchymal Stromal Cell Response. ACS Biomater. Sci. Eng. 2020, 6 (12), 6626–6651. https://doi.org/10.1021/acsbiomaterials.0c01397.

(89) Takikawa, O.; Kuroiwa, T.; Yamazaki, F.; Kido, R. Mechanism of Interferon-Gamma Action. Characterization of Indoleamine 2,3-Dioxygenase in Cultured Human Cells Induced by Interferon-Gamma and Evaluation of the Enzyme-Mediated Tryptophan Degradation in Its Anticellular Activity. J. Biol. Chem. 1988, 263 (4), 2041–2048. https://doi.org/10.1016/S0021-9258(19)77982-4.

(90) Mbongue, J. C.; Nicholas, D. A.; Torrez, T. W.; Kim, N.-S.; Firek, A. F.; Langridge, W. H. R. The Role of Indoleamine 2, 3-Dioxygenase in Immune Suppression and Autoimmunity. Vaccines 2015, 3 (3), 703–729. https://doi.org/10.3390/vaccines3030703.

(91) Däubener, W.; Wanagat, N.; Pilz, K.; Seghrouchni, S.; Fischer, H. G.; Hadding, U. A New, Simple, Bioassay for Human IFN-Gamma. J. Immunol. Methods 1994, 168 (1), 39–47. https://doi.org/10.1016/0022-1759(94)90207-0.

(92) Kwee, B. J.; Lam, J.; Akue, A.; KuKuruga, M. A.; Zhang, K.; Gu, L.; Sung, K. E. Functional Heterogeneity of IFN-γ–Licensed Mesenchymal Stromal Cell Immunosuppressive Capacity on Biomaterials. Proc. Natl. Acad. Sci. 2021, 118 (35), 1–12. https://doi.org/10.1073/pnas.2105972118.

4.0 Chapter 3: Layer-by-layer polyelectrolyte coating on Metal-organic Frameworks for use as a drug delivery device

4.0.1 Abstract

Drug delivery methods have several attributes that many accept as commonplace and unavoidable but are in fact downsides to the use of certain drugs. Many life-saving drugs suffer from these same characteristics, those being short-lifespan, poor stability, and sensitive to

temperature. Metal-organic frameworks (MOFs) have the capacity to solve each of these issues while having the added benefit of sustained release, preventing the user from needing to take multiple doses of the same drug. This is made possible by the porous nature of the framework and the interactions between the framework and the loaded drug. While research has already shown significant benefits to the use of MOFs, these interactions need to be further understood and the applications can be improved. For this reason, we present the following work in which we successfully coat the MOF UiO-66 in a layer-by-layer process using the drug heparin, commonly administered during heart attacks, and its co-factor PEI to study the effects of this new method of drug delivery using MOFs using a cytotoxicity assay. We also observe the presence and effect of the trapped cytotoxic molecule dimethylformamide as it is released from the interior of the MOF so that we can monitor the status of the outlying layers as well as monitor the release of the DMF itself. Herein, we report the successful coating of UiO-66 using polyelectrolytes and the layer-by-layer process as well as report the release of both the polyelectrolyte drug and the DMF molecules to show the methods validity as a drug delivery device.

4.0.2 Introduction

Metal-organic frameworks (MOFs) have made a significant impact on the field of chemistry in the past decade. Bringing with their popularity a vast number of functionalities and in turn applications.[21–23] The main utility of MOFs has been found in catalysis. This is due to several of their native characteristics. Those primarily being their porosity, repeating unit cell, and the vast diversity found in their components.[17,21,22,61] However, the profound effect of MOF

catalysis has outshined some of its other capabilities, one in particular being the use of a MOF as a nano-scaled delivery device.[34,74,88]

Many of the same attributes that make MOFs excellent catalytic centers also make these particles excellent carriers. Their porous nature inherently allows substances to infiltrate into the open interior space.[92,99] The charges including London dispersion forces, dipole-dipole interactions, and hydrogen bonding that occurs between the components of the framework hold the loaded substances in place and allow for controlled release to the outside environment.[28,37] Additionally, the substances (primarily proteins) trapped inside the frameworks have been shown to be protected from conditions that would otherwise cause them to deteriorate or denature. These conditions can include high or low pH, high temperature, and the presence of organic solvents[35]. The final characteristic that makes MOFs excellent carriers is their biocompatibility and their ability to elude the immune response.[128–130] Reported use of MOFs as a delivery device can be easily found in literature.[34,45,47,48,62,74,88] The coating of a MOF particle for added protection and targeted delivery has also been reported.[41,131] Each of these methods, however, has used a monolayer on the exterior of the MOF. In this work, we present for what we believe is the first time a MOF has been reported to have multiple layers. To do this, we the polyelectrolytes heparin and polyethyleneimine (PEI). The positively charged heparin is a drug commonly used to treat thrombotic events, the most well-known being atrial fibrillation or a “heart attack,” while the negatively charged PEI is a polymer commonly used in medicinal chemistry and has been shown to have little to no effect on cell viability.[132,133] Using the combination of these polymers, it is possible to use the native positive charge found on the exterior of a metal-organic framework to perform layer-by-layer

coating of the particle by introducing the negative polymer, then the positive, and alternating until the desired number of layers is achieved. Using this method, we anticipate observing the gradual release of heparin to the surrounding cellular environment while performing cell toxicity tests to monitor the effect of the heparin release on the cell in the surrounding environment. Following this, the question may arise of at what point do the exterior layers collapse and is it possible to monitor the release of a trapped carrier group from the interior of the MOF? To answer this, we intend to utilize the porous interior of the MOF to we plan to allow the presence of dimethylformamide in the interior of the MOF to determine whether the cytotoxic chemical is held in place or released through the layered system to the surrounding cells.

4.1.0 Experimental Section

4.1.1UiO-66 Synthesis

To synthesize UiO-66, we followed the procedure published by He et. al. in 2017 (CITE). In doing this, we combined 7.5g $ZrCl_4$, 5.35g of terephthalic acid, and 220 mL of acetic acid in 500 mL

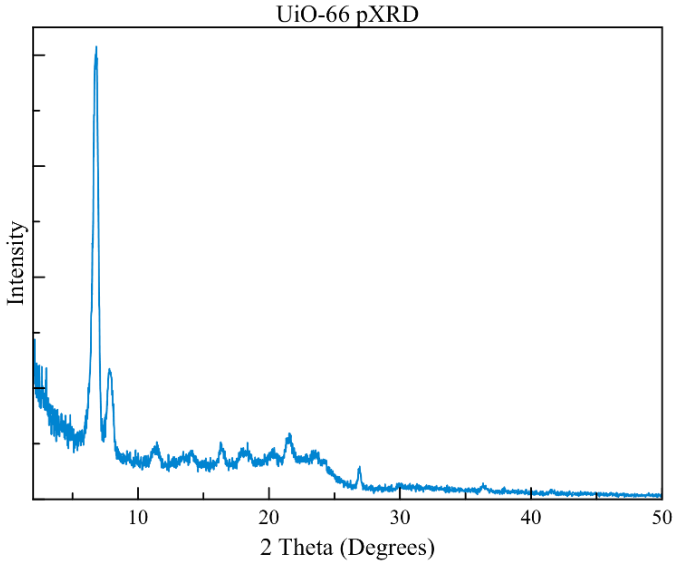

Figure 13 pXRD pf synthesized UiO-66.

DMF using a 1.0 L round bottom flask. After the components were dissolved, 35 mL of H20 was added and the reaction was allowed to progress for 15 minutes at 120°C in an oil bath. After the allotted time, the flask was removed from heat and the product was immediately separated and washed multiple times using centrifuge and alternating solvents of DMF, water, acetone, and finally hexane. Unlike the typical washing process however, the MOF was deliberately not completely cleaned. This was done so that the DMF could be trapped inside the MOF and its cytotoxic effect of cell viability could be observed and compared to the results of the coating of which its components have little to no effect (PEI) or have a promoting effect on cell viability (heparin). Confirmation of crystalline product was conducted using powder x-ray diffraction (figure 13).

4.1.2 Layer-by layer coating of UiO-66

100 mg UiO-66 was weighed out and added to 1 mL of H_2O in a 1.5 mL microcentrifuge tube. The solid particle chunks were separated using the end of a spatula before performing light sonication on the sample for 5 minutes. The solution was centrifuged at 1500 rpm for 5 minutes and the supernatant was removed. This was repeated until the supernatant was no longer cloudy. After this was observed, the liquid was removed before moving on to the coating process.

Separate solutions were then prepared with final concentrations of 1.5% PEI and 2 mg/mL Heparin. A wash solution of water was also prepared. Each solution had a final volume of 15 mL and contained 20 mM HEPES buffer stabilized at pH 7.

Next, 1 mL of the Heparin solution was added to the tube containing the UiO-66. The solution was agitated to disperse the solid and the tube was inverted for 5 minutes. The tube was

allowed to sit for 5 minutes before centrifuging the sample at 1500 rpm for 1 minute. The supernatant was then removed, and the process was repeated with the wash solution. The solution was then filled to 1 mL using the buffer solution and an aliquot was removed and set aside. This was calculated beforehand so the aliquot of this and all proceeding samples had the same MOF concentration. This cycle was completed 3 times to coat the MOF with alternating layers of Heparin, PEI, and Heparin again. Two sets of samples were made where the first set was immediately tested for size distribution (figure 17a) and proceeded to the xCELLigence test, while the second set of samples were allowed to sit at 4°C for 30 days before the solutions were removed and replaced with buffer. These samples were then tested using xCELLigence and the results were compared. The deposition of each layer was confirmed using particle size analysis on a Horiba LA-950 particle size analyzer.

4.1.4 Toxicity study: real-time monitoring of human Schwann cells cultured with HEP/PEI coated MOFs supplemented in the culture medium.

For this study we used human Schwann cells (hSCs) obtained from ATCC® (sNF96.2 ATCC® CRL-2884TM), from a male donor, 28 years old, between passages number 18 to 22 of our general stock. hSCs were cultured prior to experiments, in SIGMA-ALDRICH® Dulbecco's Modified Eagle's Medium (Cat. # D5648) supplemented with SIGMA-ALDRICH® sodium bicarbonate, sodium pyruvate, 1% penicillin-streptomycin (Cat. # P4333), and in a mixture with 10% Gibco® Fetal Bovine Serum (Cat. # 10-437-028). The cells were used only when a confluence greater than 80% was reached, after being incubated for 7 to 10 days, in a humid incubator at 37°C with an air atmosphere containing 5% CO2, with recurrent medium change every 2 days. Real-time toxicity analysis was performed using a Real-Time Cell Analyzer (RTCA) xCELLigence S16 from

ACEA Biosciences Inc. (Cat. # 00380601300) and cells were cultured in the wells of an ACEATM E-Plate 16. (Cat. # 05469830001, cell growth area 0.32 cm^2/well). All assays were done in triplicate. RTCA S16 was initially equilibrated in the incubator for 2 hours to prevent condensation from forming on the E-Plate 16 sensors. Measurements to monitor cell adhesion were performed every 10 minutes. The total time of the experiments was 144 hours (6 days). hSCs at a concentration of 25000 cells/cm2 were seeded in the microwells of E-Plate 16, initially with culture medium and after 24 hours the medium was changed and the solutions containing coated MOFs were added. Three culture medium conditions were evaluated with MOF at a concentration of 0.5 mg/mL coated with: HEP, HEP/PEI, and HEP/PEI/HEP. Also, 2 control conditions were evaluated: culture medium without MOFs and culture medium with uncoated MOFs.

4.2.0 Results & Discussion

4.2.1 UiO-66 characterization and coating.

The metal-organic framework synthesis as conducted using the previously stated method was successful, producing a white precipitate. The following XRD spectra collected matched reported results in the literature (figure 13)[134]. The coated samples were observed under TEM and several interested phenomena were observed (figure 15). In figure 15a, the bare MOF particles are isolated from one another, and no aggregation is occurring. However, when the first heparin coating is added the particles begin to aggregate (figure 15b). In contrast to this in figure 15c, the particles appear separate from one another with the formation of the poly electrolyte bilayer. In this same figure it can be observed that the

bilayer is smooth. Finally in figure 15d, the particles continue to isolate but now the outermost portion of the particle coating appears to become rough, and the layer is less defined.

It should be noted that after trial and error, it was obvious that severe agitation of the solution after the adherence of the polyelectrolyte was too violent for the complex and would strip the coating from the MOF. Therefore, any vortexing of the sample was excluded from the procedure and was instead replaced with inversions. Outside of this issue, the coating of the MOFs proceeded without any hindrance.

Using the size analyzer, the average size of the bare MOF particle and each consecutive layered particle was determined to be 0.71, 2.34, 3.01, and 3.51 µm respectively for the 0-day trial (figure 16). For the 30-day trial those values were 0.71, 1.83, 2.76, and 3.25 µm respectively. The distributions of each

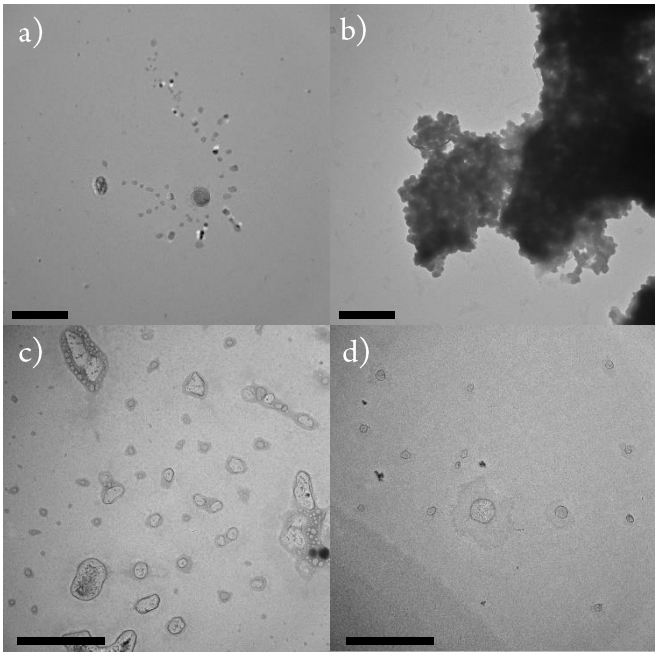

Figure 14 *SEM images of uncoated and coated MOF particles. a) uncoated UiO-66 b) UiO-66 coated with heparin c) UiO-66 coated with heparin and PEI d) UiO-66 coated with heparin, PEI, and heparin. The scale bars each represent 500 nm.*

sample were also plotted (figure 17). The coatings applied to the MOF in alternating layers of the negatively charged heparin and positively charged PEI, showed clear delineation in these graphs. This shows that the layer-by-layer coating was successfully conducted, and the polyelectrolyte layers formed

as expected.

After the 30-day period for the second set of samples, the volumes of each sample decreased by 0% for the uncoated MOF, and 38%, 16% and 14% respectively for each layer. This decrease in volume can attributed to two things. The first and simplest explanation is that as the layer sloughs off and is lost to the surrounding solution the volume of the particle decreases. The second option, that will be elaborated on more fully later in this report, is that the polyelectrolytes infiltrate into the MOF structure contributing to the loss of particle volume.

	Sample	Diameter (µm)	Volume (µm^3)	Cell Viability
0 Day Trial	MOF	0.71	0.53	65.0%
	" + Heparin	2.34	5.73	44.7%
	" + H + PEI	3.01	9.49	73.7%
	" + H + P + H	3.51	12.90	122.7%
30 Day Trial	MOF	0.71	0.53	106.3%
	" + Heparin	1.83	3.51	115.8%
	" + H + PEI	2.76	7.95	109.7%
	" + H + P + H	3.25	11.05	116.5%

Figure 15 Table showing average results from each sample set including the average cell viability normalized against the control.

4.2.2 Toxicity test

After the data was gathered from the xCElligence test and plotted, it was clear that there were 2 very different scenarios taking place in both tests. The first result that will be discussed is the trial after 30 days of refrigeration. This trial showed results that were for the most part consistent with our expectations that the layer-by-layer coatings on the MOF would either

promote cell viability due to the presence of heparin, have little to no effect with the external layer being PEI, and have a negative effect with the bare MOF. In figure18 we can see that the results follow this relative trend with the samples that had an exterior layer of heparin showing the best results promoting cell growth over the control by as much as 23.6% in the 3-layer sample, and 23.3% in the monolayered sample. In contrast, the bilayer sample only increased the cell viability by a maximum of 15.3%, while the bare MOF promoted cell viability by 9.5%. In contrast to this test, the 0-day trial yielded dramatically different results (figure 18). Starting with the 3-layer sample, the maximum cell viability was 37.4% higher than the control. After 80

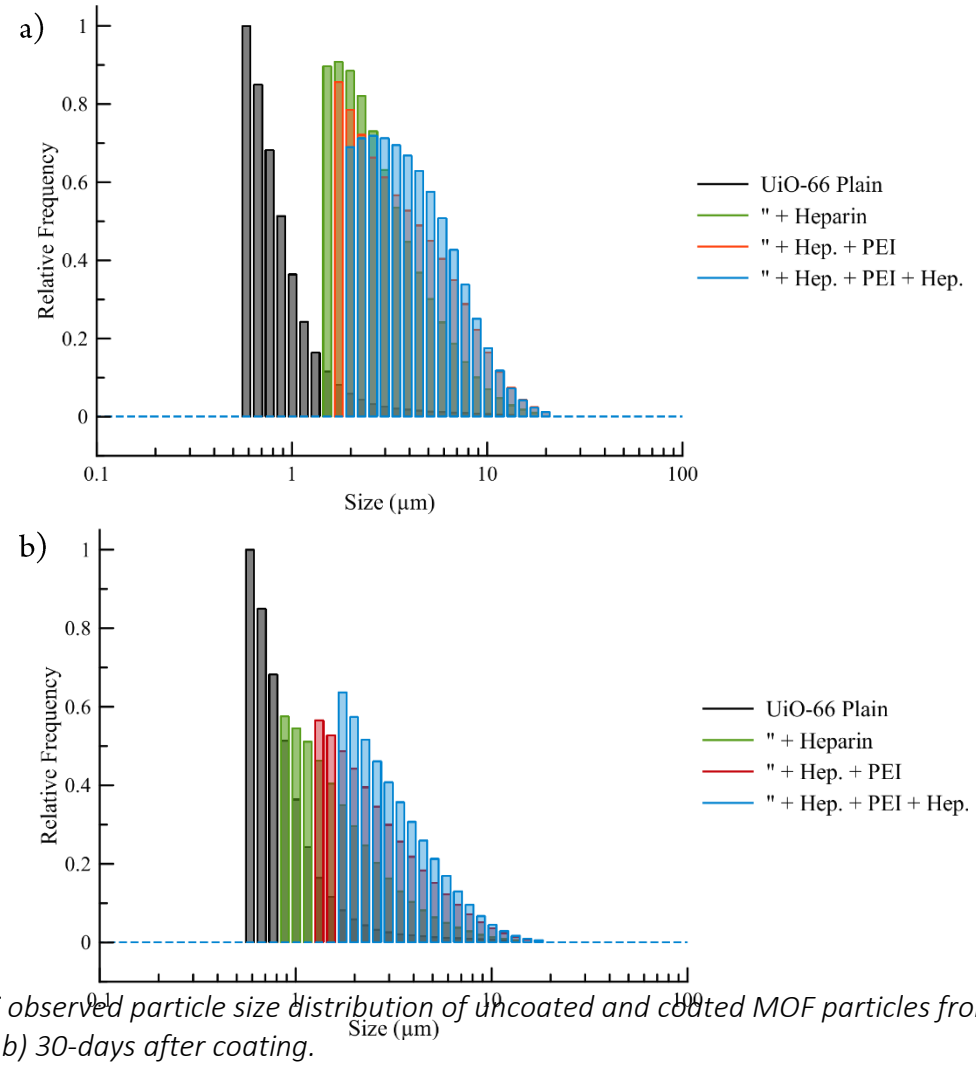

Figure 16 observed particle size distribution of uncoated and coated MOF particles from a) 0-days and b) 30-days after coating.

hours though, there began a steady decrease with the viability ended at 95.4% relative to the control. The bilayer sample had a significant increase in cell viability in the first 12 hours with a maximum cell viability of 16.1% greater than the control, but afterward continued in a steady decline of cell viability. The monolayer sample had a brief spike in cell viability, but quickly had a drastic cytotoxic effect with the percent of cells relative to the control dropping to as low as 44.7%. Surprisingly, the MOF control did not have as much of a negative effect on cell viability as the monolayered sample. Showing a cell viability minimum at 65% compared to the control. When comparing the results of these two trials it is important to remember two factors. The first being the composition of the layers themselves, and the second being the presence of the DMF that was deliberately not completely removed from the framework. When the two trials are set side-by-side, it is obvious that there is a distinct difference between the MOF control in the 0-day trial vs. the 30-day trial. This increase in cell viability after the 30-day period suggests that the DMF located in the sample leached out into solution and was removed during the wash process prior to its addition to the cells. This wash process was implemented in order to remove any excess coatings that may have sloughed off over this period but appears to have had the side-effect of also removing the cytotoxic chemical from the sample. Because of this, as well as the supporting information that nanoUiO-66 is not cytotoxic in vitro as per Rurya et. al.'s work, the results appear to suggest that the MOF itself is a promoting factor on the cell viability (figure 18) .[42] This is further supported by the fact that the bare MOF, when compared to the monolayered MOF, resulted in a higher cell viability from the 0-day trial. This result where the monolayer appears to have a negative effect on cell viability instead suggests that the heparin of the monolayer, itself not cytotoxic, either penetrated the MOF and forced out the cytotoxic

DMF or drew it out via the localized positive charge it created. Thus, leading to a “flushing” of the interior of the MOF and leading to the dramatic difference in cell viability when compared

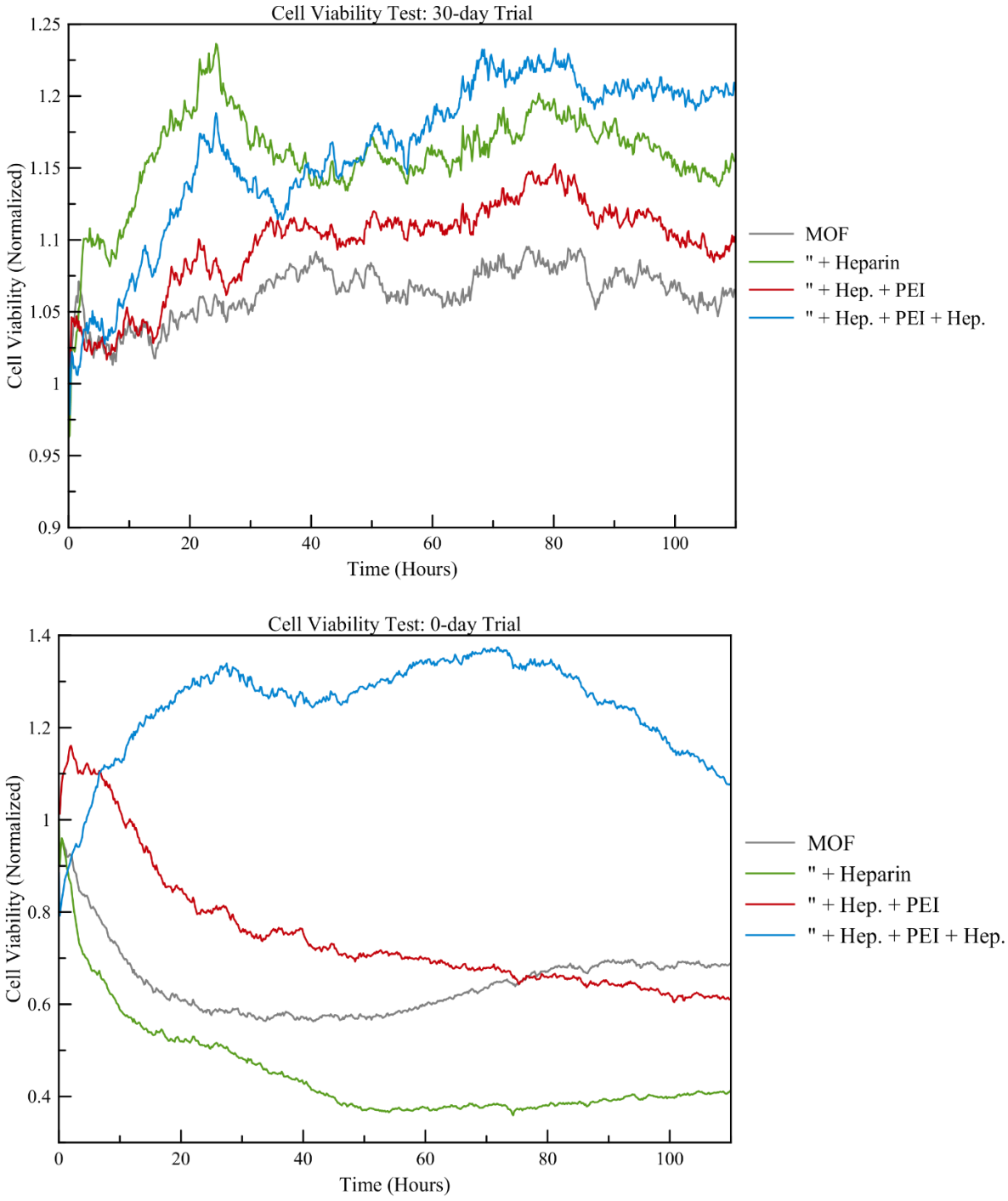

Figure 17 *Cell viability tests plotted over the course of five days using xCELLigence where (a) occurs after the samples were allowed to sit for 30 days and (b) where the samples were prepared and tested the same day. All data is normalized against the control group.*

to the bare MOF and the monolayered MOF at 30-days. Given this, it can be suggested that the same effect is occurring in the bi-layer sample, however, it appears that the effect takes longer to arise. This can be attributed to the increased size of the coating causing the release of the DMF to take longer than in the monolayer sample. In contrast to this event, the tri-layered MOF shows no cytotoxicity or any steady decrease in cell viability until 80 hours after addition. This may be due to the same effect, however, the amount of cells present suggests that the decrease in cell proliferation is more likely due to overcrowding.

4.3.0 Chapter Conclusion

In this work we utilized the MOF PCN-333(Fe) and successfully exposed it to layer-by-layer coating of the polyelectrolytes heparin and PEI as well as trapped the cytotoxic chemical dimethylformamide in order to observe the complex's effectiveness as a layer-by-layer coated delivery device. After the coating process, the complex was characterized and submitted to a cytotoxicity experiment. These results suggest that portions of the layer-by-layer coating are lost in solution over the course of 30 days, but the overall coating still remains intact. During the course of the 30-day trial, it appears that this time either allowed for the exchange and removal of DMF from inside the MOF or allowed the surrounding layers to become more ordered. This suggests that the layers are preventing the escape of the DMF. In addition to these results, in both trials the coating of heparin was found to be successfully released into the surrounding environment promoting nearby cell viability. In contrast to this, the trapped DMF in the 0-day trial showed its cytotoxic effect in the bare MOF as well as the mono-layered and bi-layered particles. Notably, there was an unexpected increase in toxicity in the mono-layered sample compared to that of the bare MOF. This result suggests that the heparin component of

the monolayer infiltrated the porous MOF and pushed out the cytotoxic DMF by nature of its negative charge into the surrounding cellular environment. The escape of DMF was evident in the cytotoxic effect present in the bi-layered sample as well, however, it took longer to be observed suggesting that the larger layer slowed its release. In this paper, we show that layer-by-layer coatings of MOF particles can be a useful tool to promote sustained release of drugs from both the exterior and the interior of MOFs including increasing the release of carried substances by the addition of a monolayer. A continuation of this research is needed to better understand these interactions and the rates at which components may be delivered.

4.4.0 References

(93) Yakushi, T.; Matsushita, K. Alcohol Dehydrogenase of Acetic Acid Bacteria: Structure, Mode of Action, and Applications in Biotechnology. Appl. Microbiol. Biotechnol. 2010, 86 (5), 1257–1265. https://doi.org/10.1007/s00253-010-2529-z.

(94) Kalscheuer, R.; Stölting, T.; Steinbüchel, A. 2006. Microdiesel: Escherichia Coli Engineered for Fuel Production. Microbiology 152 (9), 2529–2536. https://doi.org/10.1099/mic.0.29028-0.

(95) Qi, L.; Luo, Z.; Lu, X. Biomimetic Mineralization Inducing Lipase–Metal–Organic Framework Nanocomposite for Pickering Interfacial Biocatalytic System. ACS Sustain. Chem. Eng. 2019, 7 (7), 7127–7139. https://doi.org/10.1021/acssuschemeng.9b00113.

(96) Wang, H.; Han, L.; Zheng, D.; Yang, M.; Andaloussi, Y. H.; Cheng, P.; Zhang, Z.; Ma, S.; Zaworotko, M. J.; Feng, Y.; Chen, Y. Protein-Structure-Directed Metal–Organic Zeolite-like Networks as Biomacromolecule Carriers. Angew. Chem. 2020, 132 (15), 6322–6326. https://doi.org/10.1002/ange.202000299.

(97) Lian, X.; Chen, Y.-P.; Liu, T.-F.; Zhou, H.-C. Coupling Two Enzymes into a Tandem Nanoreactor Utilizing a Hierarchically Structured MOF. Chem. Sci. 2016, 7 (12), 6969–6973. https://doi.org/10.1039/C6SC01438K.

(98) Park, J.; Feng, D.; Zhou, H.-C. Dual Exchange in PCN-333: A Facile Strategy to Chemically Robust Mesoporous Chromium Metal–Organic Framework with Functional Groups. J. Am. Chem. Soc. 2015, 137 (36), 11801–11809. https://doi.org/10.1021/jacs.5b07373.

(99) Chen, W.; Yang, W.; Lu, Y.; Zhu, W.; Chen, X. Encapsulation of Enzyme into Mesoporous Cages of Metal–Organic Frameworks for the Development of Highly Stable Electrochemical Biosensors. Anal. Methods 2017, 9 (21), 3213–3220. https://doi.org/10.1039/C7AY00710H.

(100) Tani, A.; Sakai, Y.; Ishige, T.; Kato, N. Thermostable NADP+-Dependent Medium-Chain Alcohol Dehydrogenase from Acinetobacter Sp. Strain M-1: Purification and Characterization and Gene Expression InEscherichia Coli. Appl. Environ. Microbiol. 2000, 66 (12), 5231–5235. https://doi.org/10.1128/AEM.66.12.5231-5235.2000.

(101) Zhao, Q.; Hou, Y.; Gong, G.-H.; Yu, M.-A.; Jiang, L.; Liao, F. Characterization of Alcohol Dehydrogenase from Permeabilized Brewer's Yeast Cells Immobilized on the Derived Attapulgite Nanofibers. Appl. Biochem. Biotechnol. 2010, 160 (8), 2287–2299. https://doi.org/10.1007/s12010-009-8692-y.

(102) Eddaoudi, M.; Li, H.; Yaghi, O. M. Highly Porous and Stable Metal−Organic Frameworks: Structure Design and Sorption Properties. J. Am. Chem. Soc. 2000, 122 (7), 1391–1397. https://doi.org/10.1021/ja9933386.

(103) Kim, J.; Chen, B.; Reineke, T. M.; Li, H.; Eddaoudi, M.; Moler, D. B.; O'Keeffe, M.; Yaghi, O. M. Assembly of Metal−Organic Frameworks from Large Organic and Inorganic Secondary Building Units: New Examples and Simplifying Principles for Complex Structures. J. Am. Chem. Soc. 2001, 123 (34), 8239–8247. https://doi.org/10.1021/ja010825o.

(104) Eddaoudi, M.; Moler, D. B.; Li, H.; Chen, B.; Reineke, T. M.; O'Keeffe, M.; Yaghi, O. M. Modular Chemistry: Secondary Building Units as a Basis for the Design of Highly Porous and Robust Metal−Organic Carboxylate Frameworks. Acc. Chem. Res. 2001, 34 (4), 319–330. https://doi.org/10.1021/ar000034b.

(105) Wang, Q.; Astruc, D. State of the Art and Prospects in Metal–Organic Framework (MOF)-Based and MOF-Derived Nanocatalysis. Chem. Rev. 2020, 120 (2), 1438–1511. https://doi.org/10.1021/acs.chemrev.9b00223.

(106) Li, P.; Chen, Q.; Wang, T. C.; Vermeulen, N. A.; Mehdi, B. L.; Dohnalkova, A.; Browning, N. D.; Shen, D.; Anderson, R.; Gómez-Gualdrón, D. A.; Cetin, F. M.; Jagiello, J.; Asiri, A. M.; Stoddart, J. F.; Farha, O. K. Hierarchically Engineered Mesoporous Metal-Organic Frameworks toward Cell-Free Immobilized Enzyme Systems. Chem 2018, 4 (5), 1022–1034. https://doi.org/10.1016/j.chempr.2018.03.001.

(107) L. Ramos, T.; Sánchez-Abarca, L. I.; Muntión, S.; Preciado, S.; Puig, N.; López-Ruano, G.; Hernández-Hernández, Á.; Redondo, A.; Ortega, R.; Rodríguez, C.; Sánchez-Guijo, F.; del Cañizo, C. MSC Surface Markers (CD44, CD73, and CD90) Can Identify Human MSC-Derived Extracellular Vesicles by Conventional Flow Cytometry. Cell Commun. Signal. 2016, 14 (1), 2. https://doi.org/10.1186/s12964-015-0124-8.

(108) Brooke, G.; Cook, M.; Blair, C.; Han, R.; Heazlewood, C.; Jones, B.; Kambouris, M.; Kollar, K.; McTaggart, S.; Pelekanos, R.; Rice, A.; Rossetti, T.; Atkinson, K. Therapeutic Applications of Mesenchymal Stromal Cells. Semin. Cell Dev. Biol. 2007, 18 (6), 846–858. https://doi.org/10.1016/j.semcdb.2007.09.012.

(109) Pittenger, M. F.; Discher, D. E.; Péault, B. M.; Phinney, D. G.; Hare, J. M.; Caplan, A. I. Mesenchymal Stem Cell Perspective: Cell Biology to Clinical Progress. Npj Regen. Med. 2019, 4 (1), 1–15. https://doi.org/10.1038/s41536-019-0083-6.

(110) Watt, F. M.; Huck, W. T. S. Role of the Extracellular Matrix in Regulating Stem Cell Fate. Nat. Rev. Mol. Cell Biol. 2013, 14 (8), 467–473. https://doi.org/10.1038/nrm3620.

(111) Hynes, R. O. The Extracellular Matrix: Not Just Pretty Fibrils. Science 2009, 326 (5957), 1216–1219. https://doi.org/10.1126/science.1176009.

(112) Lortat-Jacob, H. The Molecular Basis and Functional Implications of Chemokine Interactions with Heparan Sulphate. Curr. Opin. Struct. Biol. 2009, 19 (5), 543–548. https://doi.org/10.1016/j.sbi.2009.09.003.

(113) Brizzi, M. F.; Tarone, G.; Defilippi, P. Extracellular Matrix, Integrins, and Growth Factors as Tailors of the Stem Cell Niche. Curr. Opin. Cell Biol. 2012, 24 (5), 645–651. https://doi.org/10.1016/j.ceb.2012.07.001.

(114) Klinker, M. W.; Marklein, R. A.; Lo Surdo, J. L.; Wei, C.-H.; Bauer, S. R. Morphological Features of IFN-γ-Stimulated Mesenchymal Stromal Cells Predict Overall Immunosuppressive Capacity. Proc. Natl. Acad. Sci. U. S. A. 2017, 114 (13), E2598–E2607. https://doi.org/10.1073/pnas.1617933114.

(115) Ijzermans, J. N.; Marquet, R. L. Interferon-Gamma: A Review. Immunobiology 1989, 179 (4–5), 456–473. https://doi.org/10.1016/S0171-2985(89)80049-X.

(116) Liu, Y.; Wang, L.; Kikuiri, T.; Akiyama, K.; Chen, C.; Xu, X.; Yang, R.; Chen, W.; Wang, S.; Shi, S. Mesenchymal Stem Cell–Based Tissue Regeneration Is Governed by Recipient T Lymphocytes via IFN-γ and TNF-α. Nat. Med. 2011, 17 (12), 1594–1601. https://doi.org/10.1038/nm.2542.

(117) Croitoru-Lamoury, J.; Lamoury, F. M. J.; Caristo, M.; Suzuki, K.; Walker, D.; Takikawa, O.; Taylor, R.; Brew, B. J. Interferon-γ Regulates the Proliferation and Differentiation of Mesenchymal Stem Cells via Activation of Indoleamine 2,3 Dioxygenase (IDO). PloS One 2011, 6 (2), e14698. https://doi.org/10.1371/journal.pone.0014698.

(118) Castilla-Casadiego, D. A.; García, J. R.; García, A. J.; Almodovar, J. Heparin/Collagen Coatings Improve Human Mesenchymal Stromal Cell Response to Interferon Gamma. ACS Biomater. Sci. Eng. 2019, 5 (6), 2793–2803. https://doi.org/10.1021/acsbiomaterials.9b00008.

(119) Zimmermann, J. A.; Hettiaratchi, M. H.; McDevitt, T. C. Enhanced Immunosuppression of T Cells by Sustained Presentation of Bioactive Interferon-γ Within Three-Dimensional Mesenchymal Stem Cell Constructs. Stem Cells Transl. Med. 2017, 6 (1), 223–237. https://doi.org/10.5966/sctm.2016-0044.

(120) Castilla-Casadiego, D. A.; Reyes-Ramos, A. M.; Domenech, M.; Almodovar, J. Effects of Physical, Chemical, and Biological Stimulus on h-MSC Expansion and Their Functional Characteristics. Ann. Biomed. Eng. 2020, 48 (2), 519–535. https://doi.org/10.1007/s10439-019-02400-3.

(121) Pinzon-Herrera, L.; Mendez-Vega, J.; Mulero-Russe, A.; Castilla-Casadiego, D. A.; Almodovar, J. Real-Time Monitoring of Human Schwann Cells on Heparin-Collagen Coatings Reveals Enhanced Adhesion and Growth Factor Response. J. Mater. Chem. B 2020, 8 (38), 8809–8819. https://doi.org/10.1039/D0TB01454K.

(122) Cifuentes, S. J.; Priyadarshani, P.; Castilla-Casadiego, D. A.; Mortensen, L. J.; Almodóvar, J.; Domenech, M. Heparin/Collagen Surface Coatings Modulate the Growth, Secretome, and Morphology of Human Mesenchymal Stromal Cell Response to Interferon-Gamma. J. Biomed. Mater. Res. A 2021, 109 (6), 951–965. https://doi.org/10.1002/jbm.a.37085.

(123) Castilla-Casadiego, D. A.; Timsina, H.; Haseli, M.; Pinzon-Herrera, L.; Chiao, Y.-H.; Wickramasinghe, S. R.; Almodovar, J. Methods for the Assembly and Characterization of Polyelectrolyte Multilayers as Microenvironments to Modulate Human Mesenchymal Stromal Cell Response. ACS Biomater. Sci. Eng. 2020, 6 (12), 6626–6651. https://doi.org/10.1021/acsbiomaterials.0c01397.

(124) Takikawa, O.; Kuroiwa, T.; Yamazaki, F.; Kido, R. Mechanism of Interferon-Gamma Action. Characterization of Indoleamine 2,3-Dioxygenase in Cultured Human Cells Induced by Interferon-Gamma and Evaluation of the Enzyme-Mediated Tryptophan Degradation in Its Anticellular Activity. J. Biol. Chem. 1988, 263 (4), 2041–2048. https://doi.org/10.1016/S0021-9258(19)77982-4.

(125) Mbongue, J. C.; Nicholas, D. A.; Torrez, T. W.; Kim, N.-S.; Firek, A. F.; Langridge, W. H. R. The Role of Indoleamine 2, 3-Dioxygenase in Immune Suppression and Autoimmunity. Vaccines 2015, 3 (3), 703–729. https://doi.org/10.3390/vaccines3030703.

(126) Däubener, W.; Wanagat, N.; Pilz, K.; Seghrouchni, S.; Fischer, H. G.; Hadding, U. A New, Simple, Bioassay for Human IFN-Gamma. J. Immunol. Methods 1994, 168 (1), 39–47. https://doi.org/10.1016/0022-1759(94)90207-0.

(127) Kwee, B. J.; Lam, J.; Akue, A.; KuKuruga, M. A.; Zhang, K.; Gu, L.; Sung, K. E. Functional Heterogeneity of IFN-γ–Licensed Mesenchymal Stromal Cell Immunosuppressive Capacity on Biomaterials. Proc. Natl. Acad. Sci. 2021, 118 (35), 1–12. https://doi.org/10.1073/pnas.2105972118.

(128) Lázaro, I. A.; Rodrigo-Muñoz, J. M.; Sastre, B.; Ángel, M. R.; Martí-Gastaldo, C.; Pozo, V. del. The Excellent Biocompatibility and Negligible Immune Response of the Titanium Heterometallic MOF MUV-10. J. Mater. Chem. B 2021, 9 (31), 6144–6148. https://doi.org/10.1039/D1TB00981H.

(129) Zhang, Y.; Wang, F.; Ju, E.; Liu, Z.; Chen, Z.; Ren, J.; Qu, X. Metal-Organic-Framework-Based Vaccine Platforms for Enhanced Systemic Immune and Memory Response. Adv. Funct. Mater. 2016, 26 (35), 6454–6461. https://doi.org/10.1002/adfm.201600650.

(130) Singh, R.; White, J. F.; de Vries, M.; Beddome, G.; Dai, M.; Bean, A. G.; Mulet, X.; Layton, D.; Doherty, C. M. Biomimetic Metal-Organic Frameworks as Protective Scaffolds for Live-Virus Encapsulation and Vaccine Stabilization. Acta Biomater. 2022, 142, 320–331. https://doi.org/10.1016/j.actbio.2022.02.002.

(131) Zhao, Q.; Li, J.; Wu, B.; Shang, Y.; Huang, X.; Dong, H.; Liu, H.; Chen, W.; Gui, R.; Nie, X. Smart Biomimetic Nanocomposites Mediate Mitochondrial Outcome through Aerobic Glycolysis Reprogramming: A Promising Treatment for Lymphoma. ACS Appl. Mater. Interfaces 2020, 12 (20), 22687–22701. https://doi.org/10.1021/acsami.0c05763.

(132) Warnock, L. B.; Huang, D. Heparin. In StatPearls; StatPearls Publishing: Treasure Island (FL), 2022.

(133) Vicennati, P.; Giuliano, A.; Ortaggi, G.; Masotti, A. Polyethylenimine in Medicinal Chemistry. Curr. Med. Chem. 2008, 15 (27), 2826–2839. https://doi.org/10.2174/092986708786242778.

(134) He, T.; Xu, X.; Ni, B.; Wang, H.; Long, Y.; Hu, W.; Wang, X. Fast and Scalable Synthesis of Uniform Zirconium-, Hafnium-Based Metal–Organic Framework Nanocrystals. Nanoscale 2017, 9 (48), 19209–19215. https://doi.org/10.1039/C7NR06274E.

5.0 Conclusion

In this paper, we aim to help develop the field's understanding of biological interactions with metal-organic frameworks. In doing this, we show that the encapsulation of the protein alcohol dehydrogenase can benefit the enzyme's catalytic action by prolonging its lifespan at room temperature showing excellent recyclability and can even be partially rejuvenated when re-introduced to refrigeration. The enzyme's activity was also protected under adverse conditions of high temperature and was even significantly increased in some scenarios such as our reaction conditions that were at a pH as low as 3 in what we refer to as an "out-of-bounds" reaction. Additionally, we show that the loading tests conducted suggest that the presence of excess buffer in solution can act as a mediating factor decreasing the interactions between the

framework and the protein. Thus, allowing the payload to increase significantly compared to the control. In line with this result, we suggest that the leaching of protein from the framework can be mitigated by the control of buffer concentration in the solution. Additionally, we found that the agitation of the complex while undergoing loading could increase the loaded material, however, this led to a decrease in activity per enzyme and suggest that a greater proportion of the proteins were not in their active state, possibly due to crowding.

In the next chapter of this work, we showed that the MOF PCN-333(Fe) also served well functioning as a delivery agent carrying INF-GAMMA to hMSC cells providing sustained release over time with no side effects to the surrounding cellular environment or the differentiation of surrounding cells. Thus, providing more support for the biocompatibility of PCN-333(Fe).

In our final chapter we showed that MOFs, specifically UiO-66, can easily be coated by a layer-by-layer coating process using polyelectrolytes up to and possibly more than 3 layers. This process successfully administered the polyelectrolyte heparin to surrounding cells and improved cell viability while the biocompatible MOF had no effect. In this work we also showed that guest substances in the interior of the framework could be released into the surrounding environment with the deterioration of the outer layers. This was done by using the cytotoxic molecule dimethylformamide and showed that the release of molecules housed in the framework could be controlled by the number of layers applied to the exterior of the MOF. In conjunction with this, we observed that a monolayer on the exterior of the MOF significantly increased the release of DMF, in a process we termed “flushing.” This effect suggests that the polyelectrolyte infiltrated the MOF and forced the DMF out using its negative charge.

In publishing these results, we aim to benefit other researchers' understanding of the interactions between biological materials and MOFs in order to advance the use of these materials in the field. The benefits of such use have so far indicated themselves as having remarkable potential which may rival conventional methods and have a significant impact in drug delivery applications. In order for this potential to be realized, research surrounding MOFs must continue. We hope that the work published here pushes the boundaries of our global knowledge on the subject and bring the application of MOFs closer to reality in biological applications.